CLINICAL REPORT

AMERICAN JOURNAL OF medical genetics PART A

Somatic *CTNNB1* Mutation in Hepatoblastoma from a Patient with Simpson–Golabi–Behmel Syndrome and Germline *GPC3* Mutation

Rika Kosaki,[1] Toshiki Takenouchi,[2] Noriko Takeda,[3,4] Masayo Kagami,[5] Kazuhiko Nakabayashi,[6] Kenichiro Hata,[6] and Kenjiro Kosaki[2,7]*

[1]Division of Medical Genetics, National Center for Child Health and Development, Tokyo, Japan

[2]Department of Pediatrics, Keio University School of Medicine, Tokyo, Japan

[3]Department of Surgery, National Center for Child Health and Development, Tokyo, Japan

[4]Department of Surgery, Kitasato University, Kanagawa, Japan

[5]Department of Molecular Endocrinology, National Research Institute of Child Health and Development, Tokyo, Japan

[6]Department of Maternal-Fetal Biology, National Research Institute of Child Health and Development, Tokyo, Japan

[7]Center for Medical Genetics, Keio University School of Medicine, Tokyo, Japan

Manuscript Received: 28 June 2013; Manuscript Accepted: 20 October 2013

Simpson–Golabi–Behmel syndrome is a rare overgrowth syndrome caused by the *GPC3* mutation at Xq26 and is clinically characterized by multiple congenital abnormalities, intellectual disability, pre/postnatal overgrowth, distinctive craniofacial features, macrocephaly, and organomegaly. Although this syndrome is known to be associated with a risk for embryonal tumors, similar to other overgrowth syndromes, the pathogenetic basis of this mode of tumorigenesis remains largely unknown. Here, we report a boy with Simpson-Golabi–Behmel syndrome who had a germline loss-of function mutation in *GPC3*. At 9 months of age, he developed hepatoblastoma. A comparison of exome analysis results for the germline genome and for the tumor genome revealed a somatic mutation, p.Ile35Ser, within the degradation targeting box of β-catenin. The same somatic mutation in *CTNNB1* has been repeatedly reported in hepatoblastoma and other cancers. This finding suggested that the *CTNNB1* mutation in the tumor tissue represents a driver mutation and that both the *GPC3* and the *CTNNB1* mutations contributed to tumorigenesis in a clearly defined sequential manner in the propositus. The current observation of a somatic *CTNNB1* mutation in a hepatoblastoma from a patient with a germline *GPC3* mutation supports the notion that the mutation in *GPC3* may influence one of the initial steps in tumorigenesis and the progression to hepatoblastoma.

Key words: hepatoblastoma; Simpson–Golabi–Behmel syndrome; CTNNB1; GPC3

How to Cite this Article:
Kosaki R, Takenouchi T, Takeda N, Kagami M, Nakabayashi K, Hata K, Kosaki K. 2014. Somatic *CTNNB1* mutation in hepatoblastoma from a patient with Simpson–Golabi–Behmel syndrome and germline GPC3 mutation.
Am J Med Genet Part A 164A:993–997.

INTRODUCTION

Simpson–Golabi–Behmel syndrome (SGBS, OMIM312870) represents an overgrowth syndrome associated with organomegaly and macroglossia accompanied by characteristic external features, such as supernumerary nipples, supernumerary ribs, hypospadias, and cryptorchidism, as well as internal malformations, such as cardiac defects, diaphragmatic hernias, and cystic dysplasia of the kidneys [Cottereau et al., 2013]. SGBS is caused by loss-of-function mutations in the heparan sulphate proteoglycan, glypican 3 gene (*GPC3*) at chromosome Xq26 [Pilia et al., 1996]. The *GPC3* gene encodes an extracellular matrix protein that is expressed during development and that regulates cell proliferation and apoptosis during

Conflict of interest: none.
Grant sponsor: Ministry of Health, Labour and Welfare, Japan the Health and Labour Sciences Research Grant for Research on rare and intractable diseases (Jitsuyoka(Nanbyo)-Ippan-003 & 13).
*Correspondence to:
Kenjiro Kosaki, M.D., Center for Medical Genetics, Keio University School of Medicine 35 Shinanomachi, Shinjuku-ku, Tokyo 160-8582, Japan. E-mail: kkosaki@z3.keio.jp
Article first published online in Wiley Online Library (wileyonlinelibrary.com): 23 January 2014
DOI 10.1002/ajmg.a.36364

development through the modulation of growth factor action, including that of IGF2 [Gonzalez et al., 1998; Pellegrini et al., 1998].

Patients with SGBS are at an increased risk for the development of embryonal tumors, such as Wilms tumor [Xuan et al., 1994; Hughes-Benzie et al., 1996; Lindsay et al., 1997] and hepatoblastoma [Lapunzina et al., 1998; Li et al., 2001; Buonuomo et al., 2005; Mateos et al., 2013]. In a recent article published in this journal, Mateos et al. [2013] documented a patient with SGBS and a *GPC3* duplication who developed a hepatoblastoma. The pathogenetic basis of the triggering and progression of embryonal tumors in the absence of a functional *GPC3* is currently unknown. Here, we document an infant with a *GPC3* mutation who developed a hepatoblastoma in which the tissue was shown to harbour a *CTNNB1* mutation using exome sequencing. This observation sheds new insight on the stepwise progression of hepatoblastoma.

CLINICAL REPORT

The propositus was born at 41 weeks of gestation as the first child of nonconsanguineous parents. He was delivered by cesarean section. His mother was 35 years old, had a height of 165 cm (+1.3 SD), and had coarse facial features. The father was 54 years old and was healthy. The birth weight of the propositus was 4,068 g (+2.65 SD), his length was 55 cm (+2.8 SD), and his head circumference was 37.5 cm (+2.66 SD). He had a ventricular septal defect that was repaired at the age of 1 month.

At the age of 4 months, his weight was 8.55 kg (+1.61 SD), his length was 68.8 cm (+1.71 SD), and his head circumference was 43.8 cm (+1.6 SD). He had an upturned bulbous nose, a wide nasal bridge, apparent hypertelorism, macrostomia, macroglossia, a midline grooved tongue, a right accessory nipple, and a short webbed neck. His hands were broad, and he had right index fingernail hypoplasia. Based on these clinical features, he was diagnosed as having SGBS (Fig. 1A). Regular surveillance was started to screen for the possible development of abdominal tumors, including hepatoblastoma and Wilms tumor. A cystic lesion was detected in the hepatic parenchyma at 9 months during an abdominal ultrasound examination. An abdominal CT scan revealed a 45 mm × 35 mm × 35 mm heterogeneously enhancing mass localized in S4 that was classified as PRETEXT stage III (Fig 1B,C). The patient's serum α-fetoprotein was elevated to 658 ng/ml. A fine needle biopsy led to a pathological diagnosis of hepatoblastoma. After chemotherapy with cisplatin and tetrahydropyranyladriamycin, the residual mass was surgically removed at the age of 14 months. At the age of 2 years, he continued to demonstrate overgrowth, with a weight of 17.1 kg (+4.58 SD) and a length of 95.7 cm (+3.4 SD).

MOLECULAR INVESTIGATION

Informed consent from the parents and approval from the institutional review board were obtained for the molecular studies. We first performed Sanger sequencing of the *GPC3* gene using DNA obtained from a peripheral blood sample of the propositus. A c.1159C > T, p.Arg387X mutation was identified, confirming the diagnosis of SGBS. Next, we obtained DNA from the hepatoblastoma tissue resected at the time of biopsy. A matched non-tumor

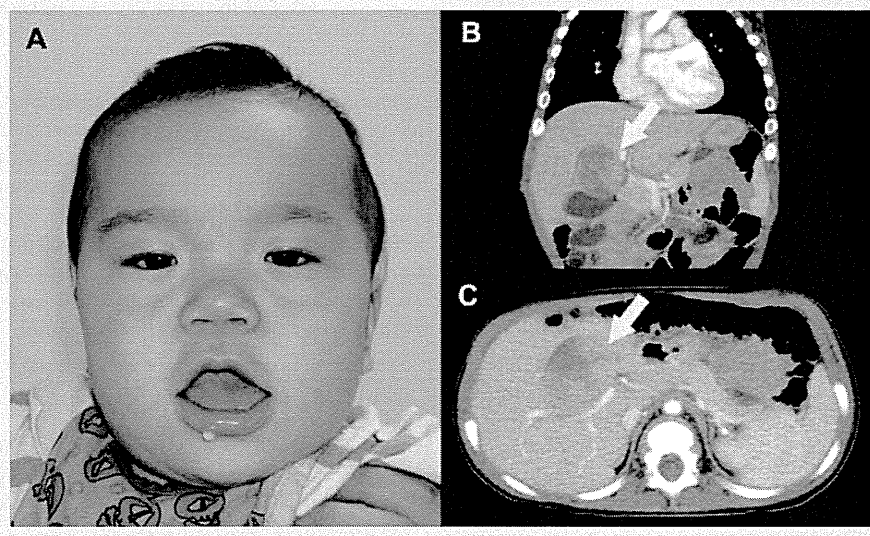

FIG. 1. The characteristic facial features and hepatoblastoma in the propositus. A: Note that the facial features of the propositus included upturned bulbous nose, a wide nasal bridge, apparent hypertelorism, macrostomia, macroglossia, and a midline grooved tongue. B and C: Coronal (B) and axial (C) slices of magnetic resonance imaging at 9 months of age showed a well-demarcated heterogeneously enhancing mass, measuring 45 mm × 35 mm × 35 mm, in S4 of the liver (yellow arrows).

peripheral blood DNA sample was also obtained. Whole-exome sequencing was performed for both DNA samples. Massive parallel sequencing on an Illumina HiSEQ platform yielded ~11 gigabases per sample, with a mean coverage of 114-fold across 54 Mb of targeted coding regions (SureSelectXT2 Human All Exon V4; Agilent Technologies, Santa Clara, CA) for each sample. The sequence reads were aligned to the reference genome assemblies (hg19) using BWA [Li and Durbin, 2009]. Local realignment around the insertions/deletions and base quality score recalibration were performed using the Genome Analysis Tool Kit software [McKenna et al., 2010], with duplicate reads removed using Picard. On average, 73% of the coding bases were covered in sufficient depth in both the tumor and the matched normal samples to allow for confident mutation detection.

MuTect version 1.14 [Cibulskis et al., 2013] was used for comparison of the exome data derived from hepatoblastoma and that derived from the peripheral blood. The default parameters were used except that max_alt_alleles_in_normal_count and minimum_mutation_cell_fraction were set to 0 and 0.1, respectively. The Mutect program detected seventy mutations as a somatic change. These 70 mutations were annotated by the program SnpEff [Cingolani et al., 2012] and classified into the following classes of mutations: non-synonymous coding, non-synonymous start, splice site acceptor, splice site donor, start lost, stop gained, and stop lost. A mutation c.104T > G, p.Ile35Ser (NM_00904) was identified at exon 3 of the *CTNNB1* that encodes β-catenin, and was the only remaining somatic mutation through the filtering process described above. This alteration was confirmed using Sanger sequencing (Fig. 2). An analysis of the reads at the mutant position after the removal of duplicated reads revealed that 72 out of 171 reads were mutant.

Mutations within a targeting box are known to lead to the accumulation of intracytoplasmic and nuclear β-catenin protein [Koch et al., 1999; Purcell et al., 2011]. The catalog of somatic mutations in cancer (COSMIC) version 64 database contained 28 instances of samples containing the somatic mutation p.Ile35Ser in *CTNNB1* under the query conditions "confirmed somatic" or "previously reported"; "tumor sample, not cultured"; and "not reported as polymorphism in the 1,000 genome projects". Out of the 29 samples, 21 originated from the liver, 2 from soft tissue, and 1 each from the endometrium, pituitary, thymus, central nervous system, and lung. Hence, most of, if not all, the samples with p.Ile35Ser were derived from the liver. Among the 21 samples, 4 samples were specifically labeled as hepatoblastoma samples; in the remaining samples, the patient's age was not mentioned, and the clinical distinction between hepatocellular carcinoma versus hepatoblastoma was not mentioned. Furthermore, a literature review on *CTNNB1* mutation analyses in hepatoblastomas in patients without multiple malformation syndromes indicated that at least five patients carried the c.104T > G, p.Ile35Ser mutation [Takayasu et al., 2001; Cairo et al., 2008; Lopez-Terrada et al., 2009; Purcell et al., 2011; Chavan et al., 2012]. The article by Takayasu et al. was not catalogued in the COSMIC database.

DISCUSSION

Through Bayesian comparison of the exome data between the germline genome and the tumor genome, we identified a somatic *CTNNB1* mutation, p.Ile35Ser, within the degradation targeting box of β-catenin in the hepatoblastoma tissue of a patient with an overgrowth syndrome, SGBS, who had a loss-of-function mutation in the *GPC3* gene.

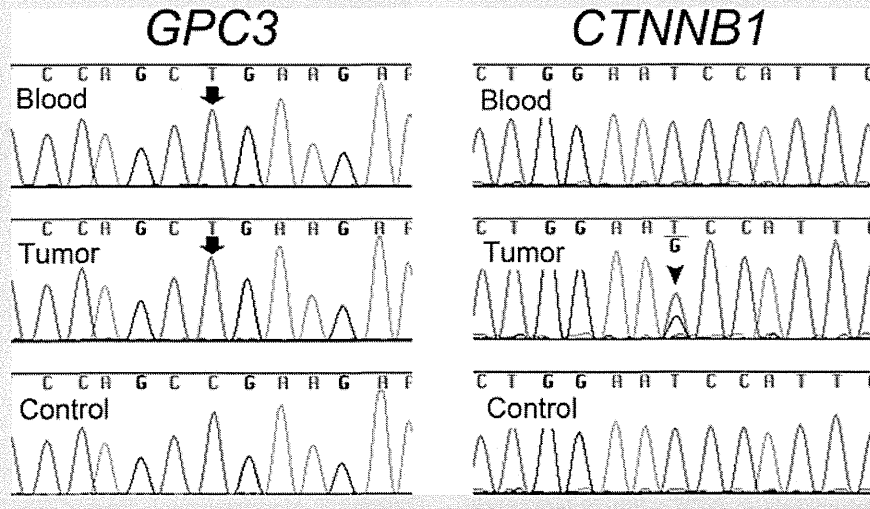

FIG. 2. Partial DNA sequences, including the sequences containing the mutations in the *GPC3* and *CTNNB1* genes. In a blood sample, a hemizygous mutation, c.1159C > T (top arrow), was identified in *GPC3*, but no mutations were identified in *CTNNB1*. In tumor tissue, a hemizygous mutation, c.1159C > T (bottom arrow), was identified in *GPC3* and a heterozygous mutation, c.104T > G (arrowhead), was identified in *CTNNB1*. The control shows a normal peripheral blood sample from a normal individual.

In general, the mutations identified in tumor tissue can be classified into two groups [Burgess, 2013]: "Driver mutations" that are directly involved in tumorigenesis followed by tumor progression, and "passenger mutations" that are not responsible for tumorigenesis or tumor progression but are by-products of genomic instability in tumor cells and are biologically neutral. A distinguishing feature of driver mutations is the recurrent appearance of the same somatic mutation in different individuals. Since the p.Ile35Ser mutation has been reported at least five times in hepatoblastomas [Takayasu et al., 2001; Cairo et al., 2008; Lopez-Terrada et al., 2009; Purcell et al., 2011; Chavan et al., 2012] and 17 times in samples from non-hepatoblastoma liver tumors, including hepatocellular carcinoma, it is reasonable to assume that the p.Ile35Ser *CTNNB1* mutation in the tumor tissue from the propositus represents a driver mutation.

The software MuTect has been shown to be efficient at detecting somatic mutations in a relatively small percentage (i.e., <10%) of tumor cells in a normal tissue background. Hence, the chance of missing mutations in other genes that are present in a subset of the cells in the tumor tissue is unlikely to be very high. Nevertheless, the classes of mutations that have been missed could include but are not limited to: (1) mutations in low coverage areas; (2) mutations in non-coding portions of the genome, such as in non-coding RNAs or regulatory elements; and (3) epigenetic changes that are undetectable using exome sequencing.

The identification of the *CTNNB1* mutation in a patient with SGBS sheds new light on the pathogenesis of hepatoblastoma: *CTNNB1* mutations within a targeting box, in which the propositus' p.Ile35Ser mutation resided, are known to lead to the accumulation of intracytoplasmic and nuclear β-catenin protein and to potentiate canonical Wnt/β-catenin signaling [Koch et al., 1999; Purcell et al., 2011]. Of note, the loss of Gpc3 leads to the activation of canonical Wnt/β-catenin signaling in *Gpc3*-knockout mice [Song et al., 2005]. If this finding is extrapolated to humans, the *GPC3* loss-of-function mutation could have exerted an additive effect on the potentiation of canonical Wnt/β-catenin signaling by the *CTNNB1* mutation. Given the fact that the propositus harbored a germline *GPC3* mutation and that the tumor harbored a somatic *CTNNB1* mutation together with the *GPC3* mutation, *GPC3* and *CTNNB1* apparently contributed to tumorigenesis in a clearly defined sequential manner, at least in the propositus. Whether mutations in *GPC3* and *CTNNB1* must occur in this specific sequence, and not vice versa, remains uncertain. Somatic loss-of-function mutations in *GPC3* have been reported in tumor tissues with various origins, including the lung (6/18), kidney (3/18), endometrium (3/18), large intestine (2/18), breast (1/18), prostate (1/18), and skin (2/18), but not in the liver according to the COSMIC database, version 66 [Forbes et al., 2011], and a search performed under the query conditions "confirmed somatic" or "previously reported"; "tumor sample, not cultured"; and "not reported" as polymorphism in the 1,000 genome projects. Hence, mutations in *GPC3* are unlikely to yield a liver-tumor-specific susceptibility to tumorigenesis or tumor progression.

From an etiological standpoint, SGBS and another prototypic overgrowth syndrome, Beckwith–Wiedemann syndrome (BWS, OMIM130650), share a key fetal growth accelerator, IGF2: the overproduction of IGF2 in BWS and the lack of an anchoring action of IGF2 by the extracellular matrix protein GPC3 in SGBS both promote fetal growth. Patients with BWS are known to have an increased susceptibility to hepatoblastoma, similar to patients with SGBS [Fukuzawa et al., 2003]. Further elucidation of the role of the *CTNNB1* mutation in hepatoblastomas in patients with BWS is warranted. Similarly, the likely role of *CTNNB1* mutation in the pathogenesis of Wilms tumor in both SGBS and BWS should be explored, together with the potential role of *GPC3* mutation in isolated hepatoblastomas.

In summary, we here document a somatic *CTNNB1* mutation in a hepatoblastoma from a patient with SGBS and a germline *GPC3* mutation. The current observation supports the notion that a mutation in *GPC3* may represent an initial step in the tumorigenesis and progression of hepatoblastoma.

ACKNOWLEDGMENTS

This work was supported by the Health and Labour Sciences Research Grant for Research on rare and intractable diseases (Jitsuyoka(Nanbyo)-Ippan-003) and Research on Applying Health Technology (H23-013) from the Ministry of Health, Labour and Welfare, Japan. We thank Ms. Yumi Obayashi for her technical assistance in article preparation.

REFERENCES

Buonuomo PS, Ruggiero A, Vasta I, Attina G, Riccardi R, Zampino G. 2005. Second case of hepatoblastoma in a young patient with Simpson-Golabi-Behmel syndrome. Pediatr Hematol Oncol 22:623–628.

Burgess DJ. 2013. Tumour evolution: Weighed down by passengers? Nat Rev Cancer 13:219.

Cairo S, Armengol C, De Reynies A, Wei Y, Thomas E, Renard CA, Goga A, Balakrishnan A, Semeraro M, Gresh L, Pontoglio M, Strick-Marchand H, Levillayer F, Nouet Y, Rickman D, Gauthier F, Branchereau S, Brugieres L, Laithier V, Bouvier R, Boman F, Basso G, Michiels JF, Hofman P, Arbez-Gindre F, Jouan H, Rousselet-Chapeau MC, Berrebi D, Marcellin L, Plenat F, Zachar D, Joubert M, Selves J, Pasquier D, Bioulac-Sage P, Grotzer M, Childs M, Fabre M, Buendia MA. 2008. Hepatic stem-like phenotype and interplay of Wnt/beta-catenin and Myc signaling in aggressive childhood liver cancer. Cancer Cell 14:471–484.

Chavan RS, Patel KU, Roy A, Thompson PA, Chintagumpala M, Goss JA, Nuchtern JG, Finegold MJ, Parsons DW, Lopez-Terrada DH. 2012. Mutations of PTCH1, MLL2, and MLL3 are not frequent events in hepatoblastoma. Pediatr Blood Cancer 58:1006–1007.

Cibulskis K, Lawrence MS, Carter SL, Sivachenko A, Jaffe D, Sougnez C, Gabriel S, Meyerson M, Lander ES, Getz G., 2013. Sensitive detection of somatic point mutations in impure and heterogeneous cancer samples. Nat Biotechnol 31:213–219.

Cingolani P, Platts A, Wang le L, Coon M, Nguyen T, Wang L, Land SJ, Lu X, Ruden DM. 2012. A program for annotating and predicting the effects of single nucleotide polymorphisms, SnpEff: SNPs in the genome of Drosophila melanogaster strain w1118; iso-2; iso-3. Fly (Austin) 6:80–92.

Cottereau E, Mortemousque I, Moizard MP, Burglen L, Lacombe D, Gilbert-Dussardier B, Sigaudy S, Boute O, David A, Faivre-Olivier L, Amiel J, Robertson R, Viana Ramos F, Bieth E, Odent S, Demeer B, Mathieu M, Gaillard D, Van Maldergem L, Baujat G, Maystadt I, Heron D, Verloes A, Philip N, Cormier-Daire V, Froute MF, Pinson L, Blanchet P, Sarda P, Willems M, Jacquinet A, Ratbi I, van den Ende J, Lackmy-Port Lis M, Goldenberg A, Bonneau D, Rossignol S, Toutain A. 2013.

Phenotypic spectrum of simpson-golabi-behmel syndrome in a series of 42 cases with a mutation in GPC3 and review of the literature. Am J Med Genet C Semin Med Genet 163C:92–105.

Forbes SA, Bindal N, Bamford S, Cole C, Kok CY, Beare D, Jia M, Shepherd R, Leung K, Menzies A, Teague JW, Campbell PJ, Stratton MR, Futreal PA. 2011. COSMIC: Mining complete cancer genomes in the catalogue of somatic mutations in cancer. Nucleic Acids Res 39:D945–D950.

Fukuzawa R, Hata J, Hayashi Y, Ikeda H, Reeve AE. 2003. Beckwith-Wiedemann syndrome-associated hepatoblastoma: Wnt signal activation occurs later in tumorigenesis in patients with 11p15.5 uniparental disomy. Pediatr Dev Pathol 6:299–306.

Gonzalez AD, Kaya M, Shi W, Song H, Testa JR, Penn LZ, Filmus J. 1998. OCI-5/GPC3, a glypican encoded by a gene that is mutated in the Simpson-Golabi-Behmel overgrowth syndrome, induces apoptosis in a cell line-specific manner. J Cell Biol 141:1407–1414.

Hughes-Benzie RM, Pilia G, Xuan JY, Hunter AG, Chen E, Golabi M, Hurst JA, Kobori J, Marymee K, Pagon RA, Punnett HH, Schelley S, Tolmie JL, Wohlferd MM, Grossman T, Schlessinger D, MacKenzie AE. 1996. Simpson-Golabi-Behmel syndrome: Genotype/phenotype analysis of 18 affected males from 7 unrelated families. Am J Med Genet 66:227–234.

Koch A, Denkhaus D, Albrecht S, Leuschner I, von Schweinitz D, Pietsch T. 1999. Childhood hepatoblastomas frequently carry a mutated degradation targeting box of the beta-catenin gene. Cancer Res 59:269–273.

Lapunzina P, Badia I, Galoppo Ç, De Matteo E, Silberman P, Tello A, Grichener J, Hughes-Benzie R. 1998. A patient with Simpson-Golabi-Behmel syndrome and hepatocellular carcinoma. J Med Genet 35:153–156.

Li H, Durbin R. 2009. Fast and accurate short read alignment with Burrows-Wheeler transform. Bioinformatics 25:1754–1760.

Li M, Shuman C, Fei YL, Cutiongco E, Bender HA, Stevens C, Wilkins-Haug L, Day-Salvatore D, Yong SL, Geraghty MT, Squire J, Weksberg R. 2001. GPC3 mutation analysis in a spectrum of patients with overgrowth expands the phenotype of Simpson-Golabi-Behmel syndrome. Am J Med Genet 102:161–168.

Lindsay S, Ireland M, O'Brien O, Clayton-Smith J, Hurst JA, Mann J, Cole T, Sampson J, Slaney S, Schlessinger D, Burn J, Pilia G. 1997. Large scale deletions in the GPC3 gene may account for a minority of cases of Simpson-Golabi-Behmel syndrome. J Med Genet 34:480–483.

Lopez-Terrada D, Gunaratne PH, Adesina AM, Pulliam J, Hoang DM, Nguyen Y, Mistretta TA, Margolin J, Finegold MJ. 2009. Histologic subtypes of hepatoblastoma are characterized by differential canonical Wnt and Notch pathway activation in DLK+ precursors. Hum Pathol 40:783–794.

Mateos ME, Beyer K, Lopez-Laso E, Siles JL, Perez-Navero JL, Pena MJ, Guzman J, Matas J. 2013. Simpson-golabi-behmel syndrome type 1 and hepatoblastoma in a patient with a novel exon 2-4 duplication of the GPC3 gene. Am J Med Genet Part A 161A:1091–1095.

McKenna A, Hanna M, Banks E, Sivachenko A, Cibulskis K, Kernytsky A, Garimella K, Altshuler D, Gabriel S, Daly M, DePristo MA. 2010. The genome analysis toolkit: A Mapreduce framework for analyzing next-generation DNA sequencing data. Genome Res 20:1297–1303.

Pellegrini M, Pilia G, Pantano S, Lucchini F, Uda M, Fumi M, Cao A, Schlessinger D, Forabosco A. 1998. Gpc3 expression correlates with the phenotype of the Simpson-Golabi-Behmel syndrome. Dev Dyn 213:431–439.

Pilia G, Hughes-Benzie RM, MacKenzie A, Baybayan P, Chen EY, Huber R, Neri G, Cao A, Forabosco A, Schlessinger D. 1996. Mutations in GPC3, a glypican gene, cause the Simpson-Golabi-Behmel overgrowth syndrome. Nat Genet 12:241–247.

Purcell R, Childs M, Maibach R, Miles C, Turner C, Zimmermann A, Sullivan M. 2011. HGF/c-Met related activation of beta-catenin in hepatoblastoma. J Exp Clin Cancer Res 30:96.

Song HH, Shi W, Xiang YY, Filmus J. 2005. The loss of glypican-3 induces alterations in Wnt signaling. J Biol Chem 280:2116–2125.

Takayasu H, Horie H, Hiyama E, Matsunaga T, Hayashi Y, Watanabe Y, Suita S, Kaneko M, Sasaki F, Hashizume K, Ozaki T, Furuuchi K, Tada M, Ohnuma N, Nakagawara A. 2001. Frequent deletions and mutations of the beta-catenin gene are associated with overexpression of cyclin D1 and fibronectin and poorly differentiated histology in childhood hepatoblastoma. Clin Cancer Res 7:901–908.

Xuan JY, Besner A, Ireland M, Hughes-Benzie RM, MacKenzie AE. 1994. Mapping of Simpson-Golabi-Behmel syndrome to Xq25-q27. Hum Mol Genet 3:133–137.

The Laryngoscope

Subgroups of Enlarged Vestibular Aqueduct in Relation to *SLC26A4* Mutations and Hearing Loss

Yasuhide Okamoto, MD; Hideki Mutai, DVM, PhD; Atsuko Nakano, MD, PhD; Yukiko Arimoto, MD, PhD; Tomoko Sugiuchi, MD; Sawako Masuda, MD; Noriko Morimoto, MD, PhD; Hirokazu Sakamoto, MD, PhD; Noboru Ogahara, MD, PhD; Akira Takagi, MD; Hidenobu Taiji, MD, PhD; Kimitaka Kaga, MD, PhD; Kaoru Ogawa, MD, PhD; Tatsuo Matsunaga, MD, PhD

Objectives/Hypothesis: To investigate possible association of hearing loss and *SLC26A4* mutations with the subgroups of enlarged vestibular aqueduct (EVA) morphology in Japanese subjects with hearing loss.

Study Design: Retrospective multicenter study.

Methods: Forty-seven subjects who had vestibular aqueduct with midpoint diameter >1 mm by computed tomography of the temporal bone were enrolled at multiple sites across Japan, and DNA samples and clinical data were collected. EVA morphology was classified into four subgroups by the pattern of enlargement: aperture, aperture and midpoint, midpoint, and borderline enlargement. Venous blood DNA samples were subjected to polymerase chain reaction–based direct sequencing of all exons and exon–intron boundaries of the *SLC26A4*.

Results: Four novel *SLC26A4* mutations were identified in the present study. *SLC26A4* mutations were detected in almost all subjects with aperture, aperture and midpoint, and midpoint enlargement. In contrast, 71% of subjects with borderline enlargement had no *SLC26A4* mutation. No significant difference was found in the distribution of truncating and nontruncating *SLC26A4* mutations between the EVA subgroups. In addition, no significant correlation was observed between the EVA subgroups and hearing levels, incidence of hearing fluctuation, or progression of hearing loss.

Conclusions: Subgroups of EVA morphology were significantly correlated with the presence or absence of *SLC26A4* mutation. In a subgroup analysis of subjects with *SLC26A4* mutations, however, differences in the EVA subgroups were not correlated with *SLC26A4* genotypes or characteristics of hearing loss.

Key Words: Enlarged vestibular aqueduct, Pendred syndrome, DFNB4, *SLC26A4*, computed tomography, hearing loss.

Level of Evidence: NA

***Laryngoscope*, 124:E134–E140, 2014**

INTRODUCTION

Enlarged vestibular aqueduct (EVA) is one of the most common inner ear deformities, often identified by computed tomography (CT) in subjects with hearing loss.[1–5] The shape and size of the EVA differ between subjects. As such, a variety of radiographic criteria to define EVA have been published. Valvassori and Clemis[6] defined EVA as a vestibular aqueduct ≥1.5 mm at the midpoint diameter. Jackler and De La Cruz[7] developed a criterion of a midpoint diameter >2.0 mm, whereas Levenson and colleagues[8] proposed a cutoff of 2.0 mm at the external aperture diameter. Okumura et al.[9] suggested an external aperture diameter >4.0 mm. Madden et al.[1] considered external aperture diameter >2.0 mm and midpoint diameter >1.5 mm as definitive, and midpoint diameter of 1.0 to 1.5 mm as borderline enlargement. Vijayasekaran et al.[10] advocated the criteria of 0.9 mm midpoint diameter or 1.9 mm external aperture diameter.

Mutations in the *SLC26A4* have been identified as a major cause of vestibular aqueduct anomalies. *SLC26A4* mutations are known to cause Pendred syndrome (Mendelian Inheritance in Man [MIM] #274600) and nonsyndromic sensorineural deafness autosomal recessive type 4 (DFNB4, MIM #600791).[11–14] Some researchers have identified a correlation between *SLC26A4* mutations, EVA, and hearing loss, whereas others report no significant relationship among *SLC26A4* genotype and these phenotypes.[15] Previous

From the Department of Otolaryngology, National Hospital Organization Tokyo Medical Center, Tokyo (Y.O., H.M., K.K., T.M.); and Department of Otorhinolaryngology, Inagi Municipal Hospital, Tokyo (Y.O.); Department of Otolaryngology, Keio University Hospital, Tokyo (Y.O., K.O.); Division of Otorhinolaryngology, Chiba Children's Hospital, Chiba (A.N., Y.A.); Department of Otolaryngology, Kanto Rosai Hospital, Kanagawa (T.S.); Department of Otorhinolaryngology, National Mie Hospital, Mie (S.M.); Department of Otorhinolaryngology, National Center for Children and Development, Tokyo (N.M., H.T.); Department of Otorhinolaryngology, Kobe Children's Hospital, Hyogo (H.S.); Department of Otorhinolaryngology, Kanagawa Children's Medical Center, Kanagawa (N.O.); Department of Otorhinolaryngology, Shizuoka General Hospital, Shizuoka (A.T.), Japan

Editor's Note: This Manuscript was accepted for publication June 27, 2013.

Supported by Health and Labor Sciences Research (Research on Rare and Intractable Diseases) grants 2009-187, 2010-205, and 2011-092, and a Grant-in-Aid for Clinical Research from the National Hospital Organization.

The authors have no other funding, financial relationships, or conflicts of interest to disclose.

Send correspondence to Tatsuo Matsunaga, MD, PhD, Department of Otolaryngology, Laboratory of Auditory Disorders, National Institute of Sensory Organs, National Hospital Organization Tokyo Medical Center, 2-5-1 Higashigaoka, Meguro, Tokyo, 152-8902, Japan. E-mail: matsunagatatsuo@kankakuki.go.jp

DOI: 10.1002/lary.24368

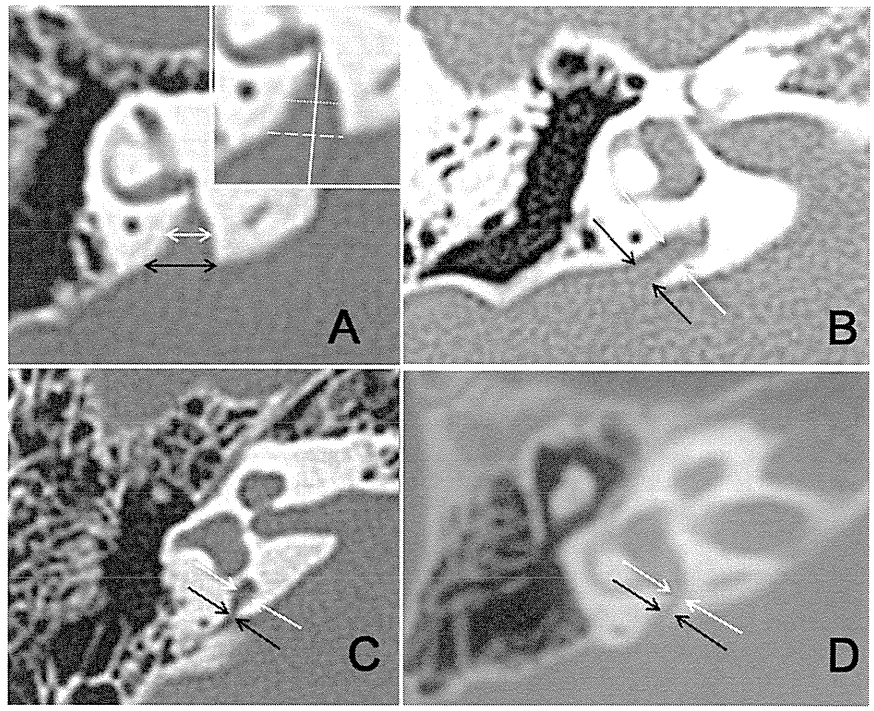

Fig. 1. Typical temporal bone computed tomographic images of the enlarged vestibular aqueduct subgroups. (A) Aperture enlargement. (B) Aperture and midpoint enlargement. (C) Midpoint enlargement. (D) Borderline enlargement. The midpoint and external aperture of the vestibular aqueduct are indicated by white and black arrows, respectively. As shown in the inset of A, the midpoint diameter (dotted line) and aperture diameter (dashed line) were measured perpendicular to the long axis (solid line) of the vestibular aqueduct.

studies have not evaluated the relationship between *SLC26A4* mutations and clinical features of hearing loss taking into consideration morphologic variations of the EVA. We conducted a multicenter study and differentiated subjects into subgroups according to vestibular aqueduct midpoint and external aperture diameters to examine a possible relationship between subgroups of EVA morphology, *SLC26A4* mutations, and hearing loss.

MATERIALS AND METHODS

We enrolled 47 bilateral EVA subjects with unilateral or bilateral sensorineural hearing loss of unknown causes (mean age = 13.5 years, range = 0–56 years; 33 children and 14 adults; 17 males and 30 females), and collected DNA samples and clinical data. Specifically, subjects whose bilateral vestibular aqueduct midpoint diameter was ≥1 mm on temporal bone CT scans were included. The midpoint and external aperture diameters were measured perpendicular to the long axis of the vestibular aqueduct on the transverse plane, as shown in the upper right-hand inset in Figure 1A. Subjects were classified into the following four subgroups based on the morphologic characteristics of the vestibular aqueduct according to the criteria in Table I: aperture enlargement, aperture and midpoint enlargement, midpoint enlargement, and borderline enlargement.

For mutation analysis, genomic DNA was extracted from venous blood and subjected to polymerase chain reaction–based direct sequencing of the exons and exon–intron boundaries of the *SLC26A4* (GenBank NG_008489). For the purpose of this study, frameshift, splice site, and nonsense mutations were categorized as "truncating," and missense mutations as "nontruncating" mutations. Novel variants were defined as pathogenic if they 1) were nonsynonymous; 2) demonstrated low carrier rates (<1%) in 96 normal control Japanese subjects, absence in database Exome Variant Server[16] and dbSNP,[17] and high amino acid conservation among various mammalian species; and 3) were detected as heterozygous in association with the other allele with another heterozygous mutation already reported as pathogenic. Alteration of splice site was predicted by NNSPLICE.[18] Subjects with *SLC26A4* mutations were analyzed for degree of hearing loss, fluctuations in hearing acuity, and progression of hearing loss to assess the relationship between these hearing parameters and EVA subgroups. Subjects underwent conditioned orientation reflex or conventional pure-tone audiometry, depending on their ages. Auditory steady-state response measurements were utilized for five subjects who did not receive any of these audiometric tests.

TABLE I.
Criteria for the Subgroups of Enlarged Vestibular Aqueduct.

Enlarged Vestibular Aqueduct Subgroup	Midpoint Diameter	External Aperture Diameter
Aperture enlargement	≥1.5 mm	Wider than midpoint
Aperture and midpoint enlargement	≥1.5 mm	Equal to midpoint
Midpoint enlargement	≥1.5 mm	Narrower than midpoint
Borderline enlargement	1.0 mm to <1.5mm	1.0 mm to <1.5 mm

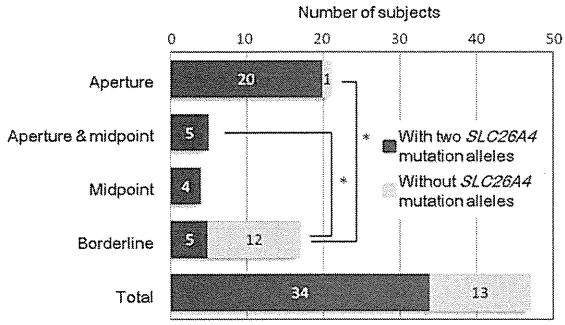

Fig. 2. Number of subjects with or without *SLC26A4* mutation alleles in each enlarged vestibular aqueduct subgroup. *Significant difference ($P < .0125$).

Hearing level was evaluated based on averages at 500, 1,000, 2,000, and 4,000 Hz (slight, 26–40 dB; moderate, 41–60 dB; severe, 61–80 dB; profound, ≥81 dB) according to the World Health Organization Grades of Hearing Impairment.[19] Subjects were considered to have fluctuating hearing loss if they had at least one bout of aggravation of hearing loss and recovery (at least 15 dB in one frequency). Subjects were considered to have progressive hearing loss if they showed aggravation of hearing loss by 10 dB or more at one or more frequencies within a 10-year interval. Statistical significance was assessed using the Fisher exact test.

All procedures were approved by the Ethics Review Committee of National Hospital Organization Tokyo Medical Center, Japan and other participating institutions, and were conducted only after written informed consent had been obtained from each subject or from the parents of the subjects.

RESULTS

Subgrouping of EVA and Its Association With SLC26A4 *Mutations*

Figure 1 shows typical CT findings in subjects with aperture enlargement (Fig. 1A), aperture and midpoint enlargement (Fig. 1B), midpoint enlargement (Fig. 1C), and borderline enlargement (Fig. 1D). Among 47 subjects, 21 (44%) were classified with aperture enlargement, 17 (36%) with borderline enlargement, five (11%) with aperture and midpoint enlargement, and four (9%) with midpoint enlargement (Fig. 2). All subjects had the same subgroup of enlargement bilaterally.

Genetic analysis of the 47 subjects showed that 34 (72%) had two *SLC26A4* mutation alleles (Table II), and the other 13 (28%) had no *SLC26A4* mutation alleles. None had a single *SLC26A4* mutation allele. The 34 subjects with two *SLC26A4* mutation alleles were diagnosed with Pendred syndrome or DFNB4. The majority of these subjects had aperture enlargement (n = 20, 59%), followed by aperture and midpoint enlargement (n = 5, 14%), borderline enlargement (n = 5, 14%), and midpoint enlargement (n = 4, 12%; Fig. 2). Conversely, most of the subjects without *SLC26A4* mutation alleles had borderline enlargement (n = 12, 91%), whereas the one remaining subject (8%) had aperture enlargement. The frequency of subjects without *SLC26A4* mutation alleles in the borderline enlargement subgroup was significantly higher than in the aperture enlargement and aperture and midpoint enlargement subgroups ($P < .0125$). It tended to be higher than in the midpoint enlargement subgroup, but this difference was not statistically significant ($P = .021$), probably due to the small number of subjects in the midpoint enlargement subgroup (n = 4).

SLC26A4 *Mutations and Genotypes in Association With EVA Morphology in Subjects With Pendred Syndrome or DFNB4*

The types and locations of all the *SLC26A4* mutations in 34 subjects with Pendred syndrome or DFNB4 are shown in Table II and Figure 3. Five splice site mutations (c.601-1G>A [intron 5], c.919-2A>G [intron 7], c.1614+1G>A [intron 14], c.1708-32_1708-16del [intron 15], c.1707+5G>A [intron 15]), one nonsense mutation (p.L743X), two insertion/deletion mutations (p.S551Ffs13, p.Q705Wfs18), and 14 missense mutations (p.S28G, p.P76S, p.A372V, p.N392Y, p.R409H, p.T410M, p.T527P, p.I529S, p.Y556C, p.V659L, p.D669E, p.F692L, p.T721M, p.H723R) were detected. These included four novel mutations, p.S28G (c.82A>G), p.D669E (c.2007C>A), p.F692L (c.2074T>C), and c.1708-32_1708-16del (marked with ** in Table II), based on the criteria for novel mutations in the present study (described in Materials and Methods). Electropherograms of the novel mutations and conservation of the amino acid residues among various species are shown in Figure 3B and C. NNSPLICE predicted c.1708-32_1708-16del to decrease the probability of an acceptor site at exon 16 from 0.49 (for a normal allele) to 0.19 (for a mutation allele), which is likely to cause aberrant splicing (Fig. 3C).

The list of subjects with two *SLC26A4* mutation alleles is shown in Table II. Analysis of genotypes of *SLC26A4* mutation alleles in these subjects showed that 20 (59%) had nontruncating/nontruncating genotypes, 13 (38%) had nontruncating/truncating genotypes, and 1 (3%) had truncating/truncating genotypes (Fig. 4A). Comparison of the incidence of each genotype found no significant statistical difference between the subgroups of EVA morphology ($P = 1.000$).

Characteristics of Hearing Loss in Association With EVA Morphology in Subjects With Pendred Syndrome or DFNB4

The hearing levels, incidence of hearing fluctuation, and progression of hearing loss in subjects with two *SLC26A4* mutation alleles are shown in Table II. The relation between the hearing level and EVA morphology was examined in the ears of 34 subjects (68 ears; Fig. 4B). Thirty-four ears (50%) had profound hearing loss in total. No significant differences in the hearing levels were detected between the subgroups of EVA morphology ($P = .462$). To exclude the effect of aging in this analysis, we also stratified the subjects into two groups (age 0–9 and ≥10 years) and conducted the same analysis. These analyses also demonstrated the same results, indicating that the difference in ages among subgroups did

TABLE II.
Types of *SLC26A4* Mutations and Characteristics of Hearing Loss in 34 Subjects With Pendred Syndrome or DFNB4 by EVA Subgroups.

			Allele 1			Allele 2						
EVA Morphology	Age at Deafness Diagnosis, yr	Age, yr	Exon/Intron	DNA Change	Amino Acid Change or Splicing Mutation	Exon/Intron	DNA Change	Amino Acid Change or Splicing Mutation	T/N	Hearing Level, R/L, dBHL*	Fluctuation of Hearing	Progression of Hearing Loss
Aperture enlargement	0	1	Intron 15	c.1707+5G>A	Splice site mutation	19	c.2106–2110dup5	p.Q705Wfs18	T/T	90/70†	–	+
	0	33	15	c.1652insT	p.S551Ffs13	19	c.2168A>G	p.H723R	T/N	95/95	–	+
	2	6	Intron 7	c.919-2A>G	Splice site mutation	19	c.2168A>G	p.H723R	T/N	53.75/63.75	–	+
	0	27	Intron 7	c.919-2A>G	Splice site mutation	19	c.2168A>G	p.H723R	T/N	98.75/100	+	+
	0	1	Intron 15	c.1707+5G>A	Splice site mutation	19	c.2168A>G	p.H723R	T/N	85‡	Unknown	+
	0	31	Intron 5	c.601-1G>A	Splice site mutation	19	c.2168A>G	p.H723R	T/N	73.75/60	+	+
	3	11	Intron 5	c.601-1G>A	Splice site mutation	19	c.2168A>G	p.H723R	T/N	70/87.5	+	+
	0	4	Intron 15	c.1707+5G>A	Splice site mutation	2	c.82A>G**	p.S28G**	T/N	61.25/61.25	–	Unknown
	0	35	Intron 5	c.601-1G>A	Splice site mutation	10	c.1229C>T	p.T410M	T/N	80/73.75	+	+
	3	12	19	c.2168A>G	p.H723R	19	c.2168A>G	p.H723R	N/N	82.5/106.25	+	+
	3	3	19	c.2168A>G	p.H723R	19	c.2168A>G	p.H723R	N/N	62.5/73.75	–	–
	0	4	19	c.2168A>G	p.H723R	19	c.2168A>G	p.H723R	N/N	55/70	+	–
	0	2	19	c.2168A>G	p.H723R	19	c.2168A>G	p.H723R	N/N	37.5‡	Unknown	Unknown
	0	1	19	c.2168A>G	p.H723R	19	c.2168A>G	p.H723R	N/N	102.5/115§	–	–
	0	0.5	10	c.1229C>T	p.T410M	19	c.2228T>A	p.L743X	N/N	73.75‡	Unknown	Unknown
	0	1	9	c.1115C>T	p.A372V	10	c.1226G>A	p.R409H	N/N	92.5‡	–	–
	0	20	19	c.2168A>G	p.H723R	14	c.1579A>C	p.T527P	N/N	97.5/101.25	–	–
	0	4	15	c.1667A>G	p.Y556C	14	c.1579A>C	p.T527P	N/N	77.5/75	–	+
	0	6	3	c.266C>T	p.P76S	14	c.1579A>C	p.T527P	N/N	17.5/93.75	–	+
	0	9	10	c.1174A>T	p.N392Y	19	c.2162C>T	p.T721M	N/N	103.75/110	+	+
Aperture and midpoint enlargement	0	15	Intron 15	c.1708-32_1708-16del**	Splice site mutation**	19	c.2168A>G	p.H723R	T/N	76.25/91.25	+	+
	0	9	Intron 7	c.919-2A>G	Splice site mutation	17	c.2007C>A**	p.D669E**	T/N	100/100	+	–
	0	1	19	c.2168A>G	p.H723R	14	c.1579A>C	p.T527P	N/N	115‡	–	–
	5	6	19	c.2168A>G	p.H723R	19	c.2168A>G	p.H723R	N/N	47.5/62.5	–	–
	1	2	19	c.2168A>G	p.H723R	19	c.2168A>G	p.H723R	N/N	105/93.75§	Unknown	Unknown
Midpoint enlargement	0	3	Intron 7	c.919-2A>G	Splice site mutation	17	c.2007C>A**	p.D669E**	T/N	82.5/93.75#	+	+
	0	8	19	c.2168A>G	p.H723R	18	c.2074T>C**	p.F692L**	N/N	75/115	+	+
	7	10	19	c.2168A>G	p.H723R	19	c.2168A>G	p.H723R	N/N	60/15	+	+
	0	35	10	c.1229C>T	p.T410M	17	c.1975G>C	p.V659L	N/N	97.5/87.5	+	+

TABLE II.
(Continued)

EVA Morphology	Age at Deafness Diagnosis, yr	Age, yr	Allele 1 Exon/Intron	Allele 1 DNA Change	Allele 1 Amino Acid Change or Splicing Mutation	Allele 2 Exon/Intron	Allele 2 DNA Change	Allele 2 Amino Acid Change or Splicing Mutation	T/N	Hearing Level, R/L, dBHL*	Fluctuation of Hearing	Progression of Hearing Loss
Borderline enlargement	0	5	Intron 7	c.919-2A>G	Splice site mutation	19	c.2168A>G	p.H723R	T/N	73.75/77.5	+	+
	2	2	Intron 14	c.1614+1G>A	Splice site mutation	10	c.1229C>T	p.T410M	T/N	55‡	Unknown	Unknown
	4	4	19	c.2168A>G	p.H723R	19	c.2168A>G	p.H723R	N/N	106.25/88.75#	Unknown	+
	0	6	14	c.1586T>G	p.I529S	19	c.2168A>G	p.H723R	N/N	80/66.25	–	–
	4	14	10	c.1229C>T	p.T410M	19	c.2168A>G	p.H723R	N/N	118.75/58.75	+	+

*Value without slash indicates binaural stimulus.
†Auditory brainstem response.
‡Conditioned Orienting Response.
**Candidate novel mutation.
§Auditory steady state response.
#Conditioned Play Audiometry.
EVA = enlarged vestibular aqueduct; L = left; N = nontruncating; R = right; T = truncating.

not affect distribution of subjects among different hearing levels (data not shown). Next, the relation between hearing fluctuation and EVA morphology was investigated in 28 subjects for whom relevant audiometric data were available (Fig. 4C). Hearing fluctuations were detected in 15 subjects (54%) in total, and no significant differences were noted in the incidence of hearing fluctuations between the subgroups of EVA morphology ($P = .209$). Lastly, the relation between progression of hearing loss and EVA morphology was analyzed in 29 subjects for whom relevant clinical data were available (Fig. 4D). Twenty subjects (69%) had progressive hearing loss in total, and the results showed no significant differences in the incidence of progressive hearing loss between the subgroups of EVA morphology ($P = .207$).

DISCUSSION

Although a variety of EVA criteria using the midpoint and aperture diameters of the vestibular aqueduct have been proposed to date,[1,6–10] our study is the first attempt to divide EVA into subgroups based on the shape and size of the vestibular aqueduct, and the first to investigate the possible relationship of these subgroups with genotypes and audiometric findings. *SLC26A4* mutations were detected in 72% of the Japanese subjects with bilateral EVA. Among these *SLC26A4* mutations, four mutations were novel. The discovery of these novel mutations would expand the *SLC26A4* mutation spectrum, thereby contributing to a more accurate gene-based diagnosis of hearing loss with EVA.

Nearly all subjects with aperture, aperture and midpoint, and midpoint enlargement presented *SLC26A4* mutations, suggesting that subjects with these EVA subgroups are most likely to be diagnosed with Pendred syndrome or DFNB4. Conversely, only approximately 30% of subjects with borderline enlargement had *SLC26A4* mutation, which suggests that the majority of subjects in this EVA subgroup have a pathological mechanism other than Pendred syndrome or DFNB4.

None of the 47 EVA subjects enrolled in the present study had only a single *SLC26A4* mutation allele. This finding is in striking contrast with previous research reporting single *SLC26A4* mutation alleles in approximately one third of Caucasian subjects with EVA.[3,4,20–22] This discrepancy might be associated with Japanese subjects, who were reported to have a spectrum of *SLC26A4* mutations distinct from that of Caucasian subjects.[22] One possible explanation is that the development of EVA in the Caucasian population may more frequently involve mutations in the introns or promoter regions of the *SLC26A4* than that in the Japanese population. Another possibility is that the Caucasian population may have higher mutation frequencies in genes than the Japanese population, causing digenic hearing loss in association with heterozygous *SLC26A4* mutations (e.g., *KCNJ10* and *FOXI1*).[23–25] The other possible explanation for the discrepancy is that the present study registered only subjects with bilateral EVA, whereas previous studies included those with unilateral hearing loss or unilateral EVA. This implicates the hypothesis that

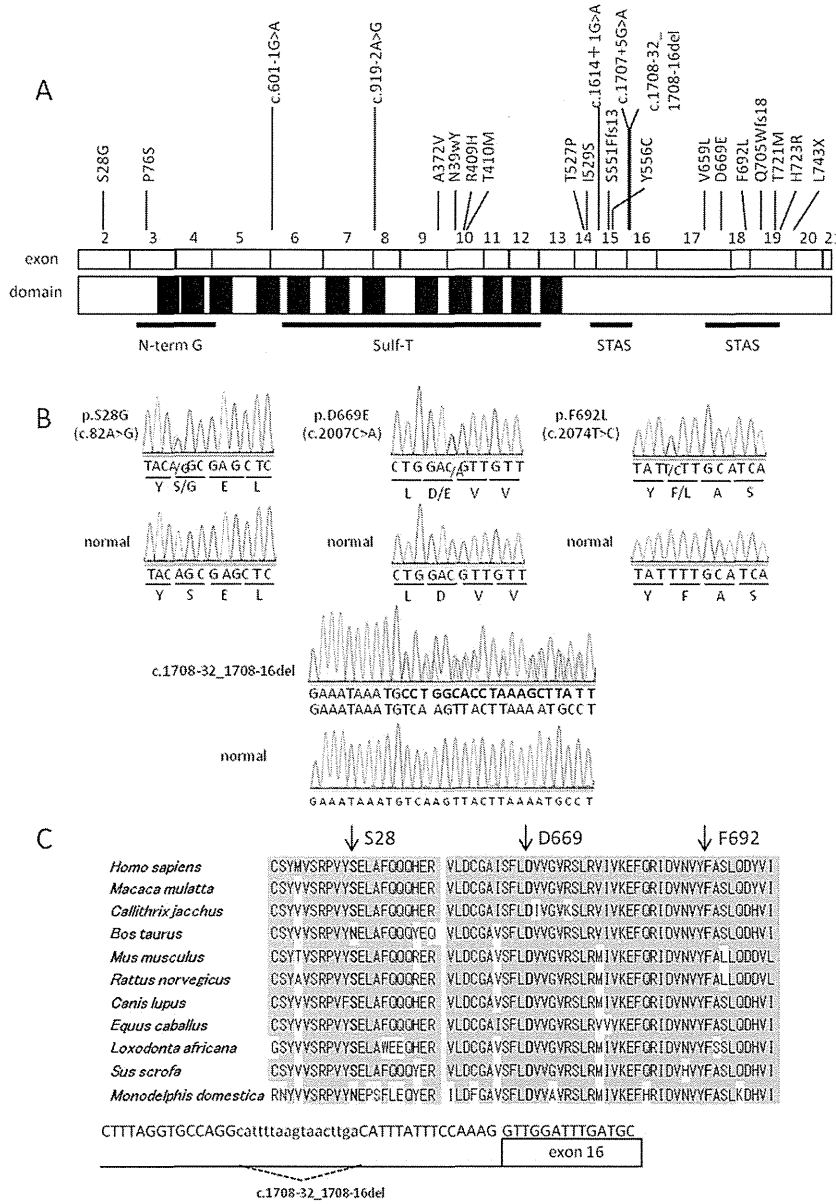

Fig. 3. The location of each mutation in *SLC26A4*, the evolutionary conservation of the amino acids, and nucleotides affected by the novel missense and splice site mutations. (A) Location of the *SLC26A4* mutations found in this study. Putative transmembrane regions are shown in black. N-term G = sulfate transporter N-terminal domain with Gly motif; STAS = sulfate transporter and anti–sigma factor antagonist domain; Sulf-T = sulfate transporter family domain. (B) electropherograms of the novel mutations and the corresponding sequence from normal alleles. Note that the nucleotide sequence of c.1708-32_1708-16del is shown reverse complementary. (C) Upper: multiple alignments of SLC26A4 protein orthologues at two noncontiguous regions. Arrows indicate affected amino acids. Conserved amino acids are shaded in gray. Lower: boundaries between intron 15 and exon 16 and deleted nucleotides are indicated at the bottom. [Color figure can be viewed in the online issue, which is available at wileyonlinelibrary.com.]

biallelic mutations of *SLC26A4* are more strongly associated with bilateral EVA.

Our analysis of subjects with *SLC26A4* mutations revealed no significant difference in the proportion of truncating and nontruncating *SLC26A4* mutations between subgroups of EVA morphology. This suggests that, in addition to malfunction of the *SLC26A4* protein, environmental factors or genes other than *SLC26A4* may contribute to variations in vestibular aqueduct morphology.

Some researchers argue that there is no significant relationship between the degree of the EVA and the severity and progression of hearing loss and hearing fluctuations, whereas others propose that there is a significant relationship.[26] In the present study, no significant differences were detected in the level, fluctuation, and progression of hearing loss between the subgroups of EVA morphology, indicating that characteristics of hearing loss cannot be predicted based on the EVA morphology in subjects with Pendred syndrome or DFNB4.

CONCLUSION

Almost all the subjects with aperture, aperture and midpoint, and midpoint enlargement of EVA had two *SLC26A4* mutation alleles, whereas more than two thirds

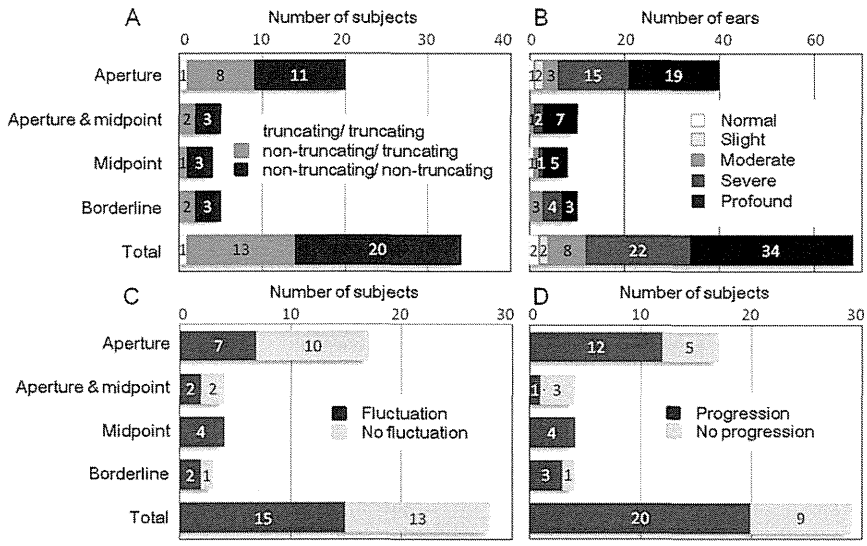

Fig. 4. Association of enlarged vestibular aqueduct (EVA) subgroups with *SLC26A4* genotypes or characteristics of hearing loss in subjects with biallelic *SLC26A4* mutations. (A) Proportion of *SLC26A4* genotypes in subjects of each EVA subgroup. (B) Proportion of different hearing levels in ears of each EVA subgroup. (C) Prevalence of fluctuating hearing loss in subjects of each EVA subgroup. (D) Prevalence of progressive hearing loss in subjects of each EVA subgroup.

of subjects with borderline enlargement of EVA had no *SLC26A4* mutation alleles. Analysis of subjects with two *SLC26A4* mutation alleles revealed no significant correlation between the morphologic subgroups of EVA and *SLC26A4* genotypes or characteristics of hearing loss, suggesting that the subgroups of EVA morphology may be associated with factors other than genotypes of *SLC26A4* mutations and that the subgroups of EVA morphology are not a predictive factor for characteristics of hearing loss.

BIBLIOGRAPHY

1. Madden C, Halsted M, Benton C, Greinwald J, Choo D. Enlarged vestibular aqueduct syndrome in the pediatric population. *Otol Neurotol* 2003; 24:625–632.
2. Madden C, Halsted M, Meinzen-Derr J, et al. The influence of mutations in the SLC26A4 gene on the temporal bone in a population with enlarged vestibular aqueduct. *Arch Otolaryngol Head Neck Surg* 2007; 133:162–168.
3. Pryor SP, Madeo AC, Reynolds JC, et al. SLC26A4/PDS genotype-phenotype correlation in hearing loss with enlarged vestibular aqueduct (EVA): evidence that Pendred syndrome and non-syndromic EVA are distinct clinical and genetic entities. *J Med Genet* 2005;42:159–165.
4. Azaiez H, Yang T, Prasad S, et al. Genotype-phenotype correlations for SLC26A4-related deafness. *Hum Genet* 2007;122:451–457.
5. Choi BY, Stewart AK, Madeo AC, et al. Hypo-functional SLC26A4 variants associated with nonsyndromic hearing loss and enlarged vestibular aqueduct: genotype-phenotype correlation or coincidental polymorphisms? *Hum Mutat* 2009;30:599–608.
6. Valvassori GE, Clemis JD. The large vestibular aqueduct syndrome. *Laryngoscope* 1978;88:723–728.
7. Jackler RK, De La Cruz A. The large vestibular aqueduct syndrome. *Laryngoscope* 1989;99:1238–1242.
8. Levenson MJ, Parisier SC, Jacobs M, Edelstein DR. The large vestibular aqueduct syndrome in children. A review of 12 cases and the description of a new clinical entity. *Arch Otolaryngol Head Neck Surg* 1989; 115:54–58.
9. Okumura T, Takahashi H, Honjo I, Takagi A, Mitamura K. Sensorineural hearing loss in patients with large vestibular aqueduct. *Laryngoscope* 1995;105:289–293.
10. Vijayasekaran S, Halsted MJ, Boston M, et al. When is the vestibular aqueduct enlarged? A statistical analysis of the normative distribution of vestibular aqueduct size. *Am J Neuroradiol* 2007;28:1133–1138.
11. Smith SD, Harker LA. Single gene influences on radiologically-detectable malformations of the inner ear. *J Commun Disord* 1998;31:391–408; quiz 409–410.
12. Everett LA, Glaser B, Beck JC, et al. Pendred syndrome is caused by mutations in a putative sulphate transporter gene (PDS). *Nat Genet* 1997;17:411–422.
13. Phelps PD, Coffey RA, Trembath RC, et al. Radiological malformations of the ear in Pendred syndrome. *Clin Radiol* 1998;53:268–273.
14. Usami S, Abe S, Weston MD, Shinkawa H, Van Camp G, Kimberling WJ. Non-syndromic hearing loss associated with enlarged vestibular aqueduct is caused by PDS mutations. *Hum Genet* 1999;104:188–192.
15. Reyes S, Wang G, Ouyang X, et al. Mutation analysis of SLC26A4 in mainland Chinese patients with enlarged vestibular aqueduct. *Am Acad Otolaryngol Head Neck Surg* 2009;141:502–508.
16. National Heart, Lung, and Blood Institute Exome Sequencing Project. Exome variant server. Available at: http://evs.gs.washington.edu/EVS/. [Visited May 13, 2013].
17. National Center for Biotechnology Information. dbSNP. Available at: http://www.ncbi.nlm.nih.gov/snp/. [Visited May 13, 2013].
18. Reese MG, Eeckman, FH, Kulp, D, Haussler, D. Improved splice site detection in Genie. *J Comp Biol* 1997;4:311–323.
19. World Health Organization. Grades of hearing impairment. Available at: http://www.who.int/pbd/deafness/hearing_impairment_grades/en/index.html. [Visited May 13, 2013].
20. Albert S, Blons H, Jonard L, et al. SLC26A4 gene is frequently involved in nonsyndromic hearing impairment with enlarged vestibular aqueduct in Caucasian populations. *Eur J Hum Genet* 2006;14:773–779.
21. Campbell C, Cucci RA, Prasad S, et al. Pendred syndrome, DFNB4, and PDS/SLC26A4 identification of eight novel mutations and possible genotype-phenotype correlations. *Hum Mutat* 2001;17:403–411.
22. Tsukamoto K, Suzuki H, Harada D, Namba A, Abe S, Usami S. Distribution and frequencies of PDS (SLC26A4) mutations in Pendred syndrome and nonsyndromic hearing loss associated with enlarged vestibular aqueduct: a unique spectrum of mutations in Japanese. *Eur J Hum Genet* 2003;11:916–922.
23. Madeo AC, Manichaikul A, Reynolds JC, et al. Evaluation of the thyroid in patients with hearing loss and enlarged vestibular aqueducts. *Arch Otolaryngol Head Neck Surg* 2009;135:670–676.
24. Yang T, Vidarsson H, Rodrigo-Blomqvist S, Rosengren SS, Enerback S, Smith RJ. Transcriptional control of SLC26A4 is involved in Pendred syndrome and nonsyndromic enlargement of vestibular aqueduct (DFNB4). *Am J Hum Genet* 2007;80:1055–1063.
25. Yang T, Gurrola JG Jr, Wu H, et al. Mutations of KCNJ10 together with mutations of SLC26A4 cause digenic nonsyndromic hearing loss associated with enlarged vestibular aqueduct syndrome. *Am J Hum Genet* 2009;84:651–657.
26. Gopen Q, Zhou G, Whittemore K, Kenna M. Enlarged vestibular aqueduct: review of controversial aspects. *Laryngoscope* 2011;121:1971–1978.

Gene 540 (2014) 258–262

Contents lists available at ScienceDirect

Gene

journal homepage: www.elsevier.com/locate/gene

Short Communication

Chronic constipation recognized as a sign of a *SOX10* mutation in a patient with Waardenburg syndrome

Yukiko Arimoto [a], Kazunori Namba [b], Atsuko Nakano [a], Tatsuo Matsunaga [b,*]

[a] Division of Otolaryngology, Chiba Children's Hospital, Japan
[b] Laboratory of Auditory Disorders, National Institute of Sensory Organs, National Tokyo Medical Center, Japan

ARTICLE INFO

Article history:
Accepted17 February 2014
Available online 28 February 2014

Keywords:
SOX10
Waardenburg syndrome
Chronic constipation
Hirschsprung disease
Inner ear malformation

ABSTRACT

Waardenburg syndrome is characterized by hearing loss, pigmentation abnormalities, dysmorphologic features, and neurological phenotypes. Waardenburg syndrome consists of four distinct subtypes, and *SOX10* mutations have been identified in type II and type IV. Type IV differs from type II owing to the presence of Hirschsprung disease. We identified a de novo nonsense mutation in *SOX10* (p.G39X) in a female pediatric patient with Waardenburg syndrome with heterochromia iridis, profound bilateral sensorineural hearing loss, inner ear malformations, and overall hypopigmentation of the hair without dystopia canthorum. This patient has experienced chronic constipation since she was a neonate, but anorectal manometry showed a normal anorectal reflex. Chronic constipation in this patient was likely to be a consequence of a mild intestinal disorder owing to the *SOX10* mutation, and this patient was considered to have a clinical phenotype intermediate between type II and type IV of the syndrome. Chronic constipation may be recognized as indicative of a *SOX10* mutation in patients with Waardenburg syndrome.

1. Introduction

Waardenburg syndrome (WS) is a hereditary disease characterized by sensorineural hearing loss and pigmentation abnormalities that is classified into four subtypes according to clinical symptoms (Read and Newton, 1997). WS with dystopia canthorum (W index > 1.95) is classified as WS type I (WS1), WS without dystopia canthorum as type II (WS2), WS with symptoms of WS1 and musculoskeletal abnormalities in the upper extremities as type III (WS3), and WS with symptoms of WS2 and Hirschsprung disease as type IV (WS4). In addition, WS is genetically heterogeneous (Pingault et al., 2010). There are eight confirmed loci (viz., WS1/WS3 on 2q36.1, WS2A on 3p14.1-p12.3, WS2B on 1p21-p13.3, WS2C on 8p23, WS2D on 8q11.21, WS2E/WS4C on 22q13.1, WS4A on 13q22.3 and WS4B on 20q13.2-q13.3) and six known genes (viz., *PAX3* for WS1/WS3, *MITF* for WS2A, *SNAI2* for WS2D, *SOX10* for WS2E/WS4C, *EDNRB* for WS4A and *EDN3* for WS4B loci) for WS (Kapoor et al., 2012). Mutations in *SOX10* were first reported in WS4 and later in WS2 (Bondurand et al., 2007; Pingault et al., 1998). WS4 accompanied by neurological symptoms owing to insufficient myelination of central or peripheral nerves is called peripheral demyelinating neuropathy, central dysmyelinating leukodystrophy, Waardenburg syndrome, and Hirschsprung disease (PCWH), and PCWH is also associated with *SOX10* mutations (Inoue et al., 1999). In addition, *SOX10* mutations have been identified in patients with WS2 with similar neurological symptoms (Barnett et al., 2009). Some patients with WS with *SOX10* mutations have intestinal pseudo-obstruction with symptoms of ileus despite the presence of enteric ganglia (Elmaleh-Bergès et al., 2012; Pingault et al., 2002).

In this study, we report a 3-year-old girl who presented with chronic constipation as well as hearing loss, inner ear malformations, and pigmentation abnormalities. Her condition was considered to be a clinical phenotype intermediate between type II and type IV of the syndrome, and suggested that chronic constipation may be a sign of a *SOX10* mutation in patients with WS.

2. Materials and methods

2.1. Clinical evaluation

All the procedures were approved by the Ethics Review Committee of National Tokyo Medical Center and Chiba Children's Hospital, and were carried out only after a written informed consent had been obtained from each individual or parents of the child.

Abbreviations: WS, Waardenburg syndrome; ABR, auditory brainstem response; PCWH, peripheral demyelinating neuropathy, central dysmyelinating leukodystrophy, Waardenburg syndrome, and Hirschsprung disease; *CT*, computed tomography; NMD, nonsense-mediated mRNA decay.

* Corresponding author at: Laboratory of Auditory Disorders and Department of Otolaryngology, National Institute of Sensory Organs, National Tokyo Medical Center, 2-5-1 Higashigaoka, Meguro, Tokyo 152-8902, Japan.
E-mail address: matsunagatatsuo@kankakuki.go.jp (T. Matsunaga).

http://dx.doi.org/10.1016/j.gene.2014.02.041
0378-1119/

Hearing loss in the proband was assessed by auditory brainstem response (ABR) and play audiometry. Malformations of the inner ear were assessed by computed tomography (CT) of the temporal bone. During the recording sessions for ABR and CT, the patient was in a state of induced sleep with triclofos sodium (80 mg/kg, administered orally). ABR studies were obtained using the Neuropack device (Nihonkohden Corporation, Tokyo, Japan). Play audiometry was performed by an Audiometer AA-75 (Rion, Tokyo, Japan). Based on pure-tone air-conduction thresholds, the degree of hearing loss was determined by the better ear pure-tone average across the frequencies 0.5, 1, 2, and 4 kHz, and it was classified as mild (20–40 dB), moderate (41–70 dB), severe (71–95 dB), or profound (>95 dB) according to the recommendations for the description of audiological data by the Hereditary Hearing Loss Homepage (http://hereditaryhearingloss.org). CT was conducted using a LightSpeed VCT 64-slice scanner (GE Healthcare, CT, USA). Anorectal reflex was measured by a Anorectal reflex monitor Pocket monitor (Star Medical, Tokyo, Japan).

2.2. Gene analysis

Genomic DNA was extracted from blood samples using the Gentra Puregene Blood kit (QIAGEN, Venlo, Netherlands), and primers specific for *SOX10* (GenBank NG_007948.1) (http://www.ncbi.nlm.nih.gov/Genbank/) were designed. For PCR amplification of *SOX10* exons 1, 2 and 3, the primer sets 5′-TGTAAAACGACGGCCAGTagatgggtttagctggagca-3′, and 5′-CAGGAAACAGCTATGACCaatccacccgaagctagagg-3′, and 5′-TGTAAAACGACGGCCAGTtctcaccctccagcccatga-3′, and 5′-CAGGAAACAGCTATGACCtgccatccagccatctcctg-3′, and 5′-TGTAAAACGACGGCCAGTcccgactcatgctgccaaa-3′, and 5′-CAGGAAACAGCTATGACCcccgacctgtcagcctcttca-3′ were used with the PC-818 Program Temp Control System (Advanced Science and Technology Enterprise Corporation, Tokyo, Japan). Each primer is specific for a given genomic sequence (lower case) and was used in combination with either a universal forward M13 (upper case) or reverse M13pUC (upper case) primer. The following PCR program was used: 98 °C for 5 min; 35 cycles of 98 °C for 10 s, 62 °C for 10 s, and 72 °C for 1.2 min; and then 72 °C for 3 min. PrimeSTAR HS DNA polymerase (Takara Bio, Shiga, Japan) was used for the PCR. The amplicons were sequenced using the ABI 3730 DNA sequence analyzer with the ABI Prism Big Dye Terminator Cycle Sequencing kit (Applied Biosystems, CA, USA).

3. Results

3.1. Clinical features

A 3-year-old girl born to a Japanese mother and a Chinese father was referred to our hospital with the chief complaint of unstable neck at the age of 4 months. She did not have any prenatal abnormalities. Her irises were light blue and her hair was mostly brown. When hearing acuity was tested by ABR, the wave V threshold was 105dBnHL for the right ear, and the left ear did not respond to the sound of 105dBnHL. No dystopia canthorum was observed. Based on these clinical features, she was first suspected to have WS2. No other members of her family had similar symptoms (Fig. 1). Play audiometry at 2 years and 10 months of age revealed bilateral profound sensorineural hearing loss (Fig. 2). CT of the temporal bone revealed hypoplastic cochleae in which the first turn and the second turn were not separated (Figs. 3A, B, arrows), and the cochlear nerve canal was intercepted by a bony plate (Figs. 3C, D, arrows) in both ears. The vestibule was enlarged in both ears (Figs. 3E, F). Arches of the superior and lateral semicircular canals were also enlarged near the vestibule. The posterior semicircular canal was absent, and potential anlagen of the posterior semicircular canal were visible in both ears (Figs. 3E, F; arrows). The vestibular aqueduct was normal in both ears.

Meconium passage was noted within 24 h of birth, but chronic constipation subsequently occurred. The patient did not experience a natural bowel movement for periods of 5 days or longer, and thus stimulant laxatives were administered to the patient daily. Anorectal manometry confirmed a normal anorectal reflex, indicating the presence of enteric ganglia (Fig. 4). No neurological symptoms indicative of neuropathy were noted.

3.2. Genetic features

Given the patient's clinical manifestations, she was suspected of having WS2 or WS4. Thus, *MITF* and *SOX10* were initially analyzed. The DNA of the patient and particular family members (Fig. 1) were extracted from venous blood, and all *MITF* and *SOX10* coding exons and their flanking intronic sequences were amplified using polymerase chain reaction (PCR; primer sequences and PCR conditions are available upon request). DNA sequencing of these PCR products did not reveal any mutations in *MITF*, but a heterozygous *SOX10* mutation of c. 115G>T

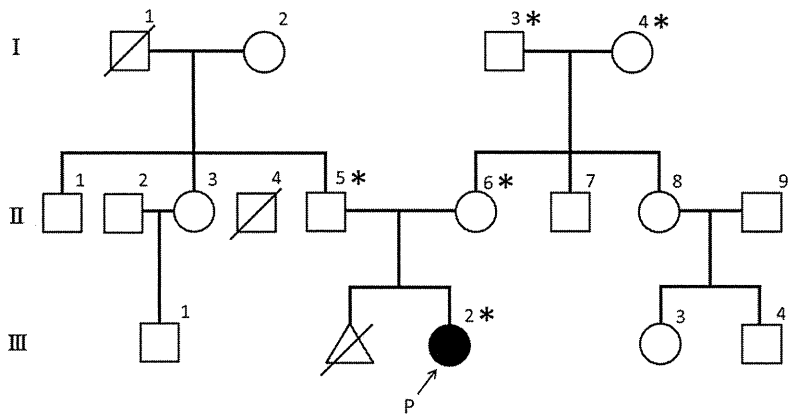

Fig. 1. Family pedigree of the family. Individuals who were examined and whose blood samples were collected for DNA analysis are indicated by asterisks. Only the proband (P) had the characteristic symptoms indicating WS, and no other familial members had similar symptoms. The pedigree was described in the style that followed "Recommendations for standardized human pedigree nomenclature" (Bennett et al., 1995). Roman numerals indicate generations of the family and individuals are numbered for identification by Arabic numerals in each generation. Open squares and open circles indicate unaffected males and unaffected females, respectively. Crossed squares and a crossed triangle represent deceased males and an abortion, respectively. A filled circle indicates a female affected with WS.

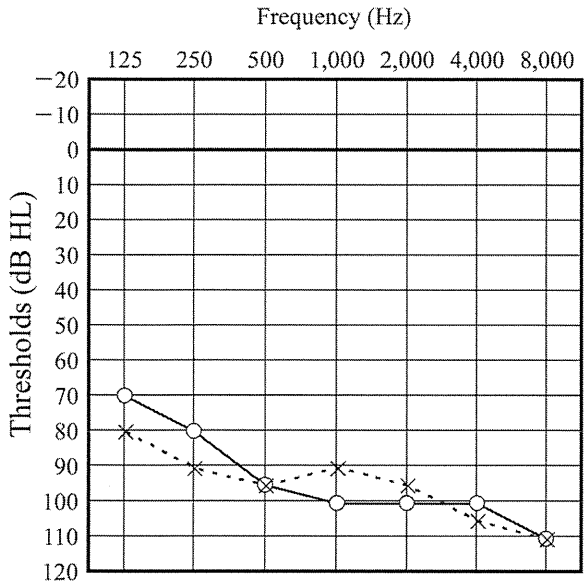

Fig. 2. Play audiometry of the patient. Pure tone thresholds of the right ear are indicated with "○", and those of the left ear are indicated with "×". It was shown that the patient had bilateral profound hearing loss according to the definitions of the degree of hearing loss described in the Materials and methods.

(p.G39X) was identified in the patient (Fig. 5). This mutation was not found in the parents, maternal grandparents, or the control group which consisted of 96 unrelated Japanese individuals with normal hearing as determined with pure tone audiometry.

4. Discussion

The present patient had WS with a confirmed de novo *SOX10* nonsense mutation and presented with chronic constipation. Although Hirschsprung disease and intestinal pseudo-obstruction have been reported in association with WS4, the chronic constipation observed in this patient did not fit these profiles. There have been two reported patients who presented constipation in WS associated with *SOX10* mutations (Chaoui et al., 2011). However, unlike the patient in the present study, those two patients had clinical phenotype of peripheral demyelinating neuropathy, central dysmyelinating leukodystrophy, and WS or PCWH which are associated with peripheral demyelinating neuropathy and central dysmyelinating leukodystrophy and such neurological phenotypes suggest *SOX10* mutations by themselves without constipation. In addition, constipation in the two patients could be caused by central dysmyelinating leukodystrophy. Therefore, their constipation may not be caused by the abnormality in enteric ganglia due to *SOX10* mutations.

On the other hand, the present patient was absent from the neurological phenotypes, and considered as having a clinical phenotype intermediate between WS2 and WS4. Because WS2 and WS4 have several causative genes including *MITF*, *SOX10*, *EDN3*, *EDNRB*, and *SNAI2*, constipation was the only phenotype suggesting *SOX10* mutations among those candidate

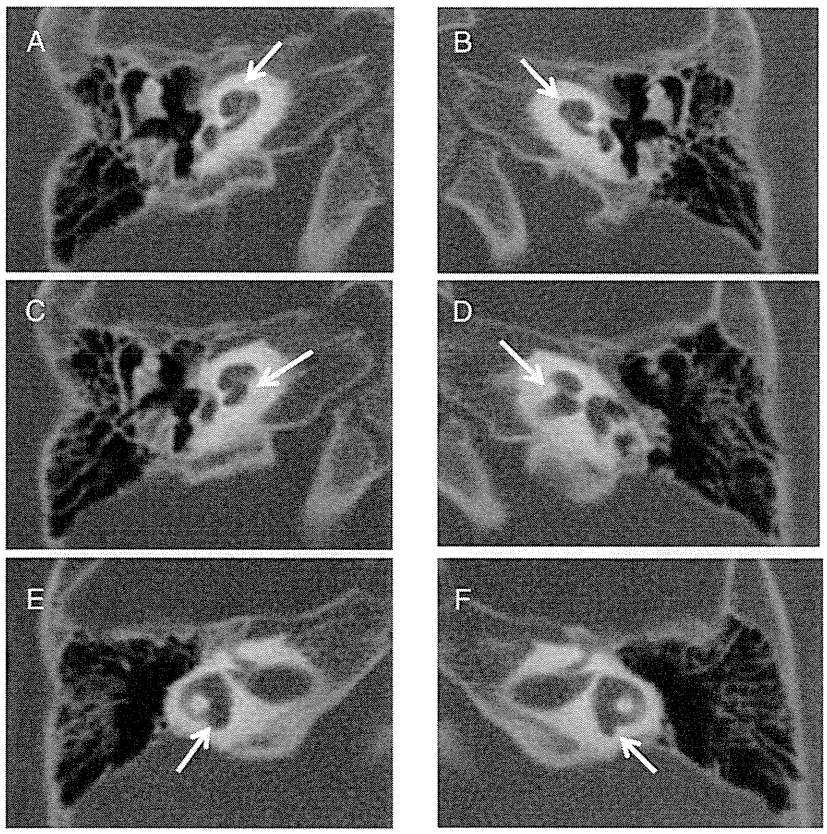

Fig. 3. CT of the temporal bone of the patient. The right ear is shown in the left column (A, C, E), and the left ear is shown in the right column (B, D, F). Each row shows the same level of horizontal section of the inner ear. Bilateral inner ear malformations of this patient are shown in these images. Hypoplasia of the bilateral cochleae (A, B; arrows). Atresia of the bilateral cochlear nerve canals (C, D; arrows). Enlarged vestibules with potential anlagen of the posterior semicircular canals (E, F; arrows).

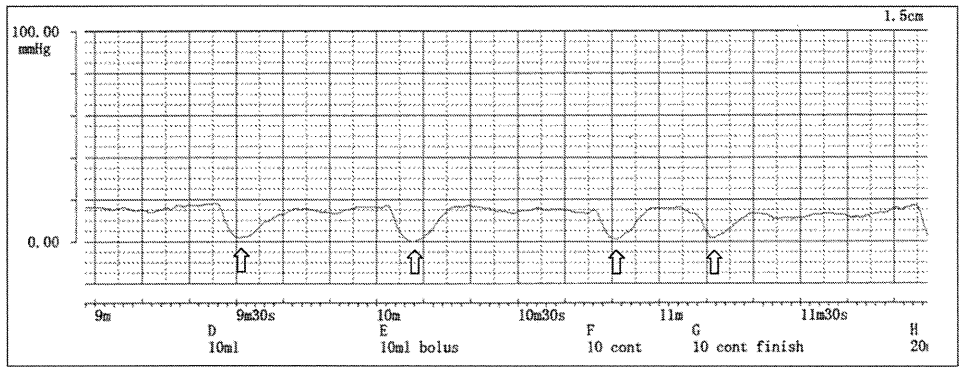

Fig. 4. Anorectal manometry of the patient. Anorectal pressure plots along the perpendicular axis and time course plots along the horizontal axis. A normal anorectal reflex (indicated with upward-pointing arrows) was confirmed repeatedly in this patient.

genes in the present patient. In addition, because the present patient did not have the neurological phenotypes, constipation in this patient was likely to be caused by abnormality in enteric ganglia, which suggested

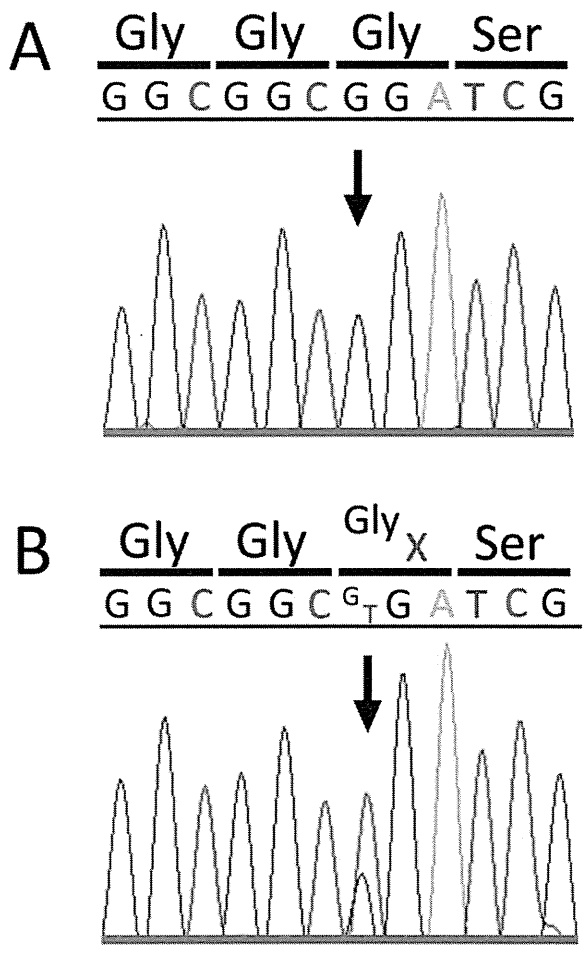

Fig. 5. Sequence chromatogram of *SOX10*. A: In the control, a homozygous G indicated by an arrow is the first nucleotide of the codon 39 for glycine (Gly). B: In the proband, a heterozygous G to T transition (arrow) at the same position leads to replacement of glycine (Gly) at the codon 39 with a stop codon (X), which causes premature termination of protein synthesis.

SOX10 mutations. Thus, the present patient demonstrated additional clinical significance of constipation in WS, and suggested that chronic constipation may be an important clinical sign of *SOX10* mutations in patients with WS, especially those without the neurological phenotypes.

Sham et al. (2001) examined the relationship between *SOX10* mutation sites and the severity of Hirschsprung disease by analyzing patients reported in the literature as well as their own patients. Patients with nonsense mutations in upstream regions of *SOX10* had aganglionosis only in short regions of the intestine that manifested as mild Hirschsprung disease, whereas patients with nonsense mutations in the last exon had aganglionosis along the entire colon and severe Hirschsprung disease. According to Inoue et al. (2004), in diseases with a dominant inheritance pattern, when a nonsense mutation is located 50 bases or more upstream of the last exon–exon junction, nonsense-mediated mRNA decay (NMD) occurs and causes haploinsufficiency, leading to a mild phenotype. In contrast, a nonsense mutation located in a region where NMD does not occur induces a dominant-negative effect and results in a severe phenotype. The p.G39X mutation in this patient was the most upstream nonsense mutation among those reported to date. Therefore, the mild phenotype in this patient is likely due to haploinsufficiency caused by NMD.

The other reported patients with the mutation in the same region of *SOX10* also presented with mild intestinal features (Pingault et al., 2002; Sham et al., 2001). A patient carried a nonsense mutation (p.R43X), and another patient carried a frameshift mutation (p.E57SfsX52). Both patients were affected with Hirschsprung disease, and found to have aganglionosis in a short segment of the intestine. We hypothesize that intestinal disorders owing to *SOX10* mutations can be viewed as a continuum: (1) with severe effects, the absence of enteric ganglion cells leads to severe Hirschsprung disease, especially with aganglionosis in long segment; (2) with moderate effects, Hirschsprung disease becomes mild type with aganglionosis in short segment, or, enteric ganglion cells are present, but intestinal pseudo-obstruction develops and causes symptoms similar to those of Hirschsprung disease; and (3) with mild effects, enteric ganglion cells are present and only chronic constipation may occur. Chronic constipation, which is a common clinical symptom that can easily be overlooked when it is mild, may be indicative of a *SOX10* mutation in patients with WS.

The present patient also had inner ear malformations. WS can be accompanied by inner ear malformations in some cases (Madden et al., 2003; Oysu et al., 2001). A recent study found inner ear malformations in patients with WS2, WS4, and PCWH with confirmed *SOX10* mutations (Elmaleh-Bergès et al., 2012). According to this study, all 15 patients examined had absent, abnormally shaped, or abnormally sized bilateral semicircular canals. No abnormalities were observed in the cochleae of 13 of the 15 patients. Because abnormalities were

found in the lateral semicircular canal in 100% of these patients, in the posterior semicircular canal in 93%, and in the superior semicircular canal in 87%, bilateral malformations in semicircular canals are considered to be indicative of WS that is associated with *SOX10* mutations. The patient in the present study was consistent with the proposed relationship between the inner ear malformation and *SOX10* mutations.

Conflict of interest

None.

References

Barnett, C.P., et al., 2009. Aplasia of cochlear nerves and olfactory bulbs in association with SOX10 mutation. American Journal of Medical Genetics Part A 149A, 431–436.
Bennett, R.L., et al., 1995. Recommendations for standardized human pedigree nomenclature. American Journal of Human Genetics 56, 745–752.
Bondurand, N., et al., 2007. Deletions at the SOX10 gene locus cause Waardenburg syndrome types 2 and 4. American Journal of Human Genetics 81, 1169–1185.
Chaoui, A., et al., 2011. Identification and functional analysis of SOX10 missense mutations in different subtypes of Waardenburg syndrome. Human Mutation 32, 1436–1449.
Elmaleh-Bergès, M., et al., 2012. Spectrum of temporal bone abnormalities in patients with Waardenburg syndrome and SOX10 mutations. American Journal of Neuroradiology 34, 1257–1263.
Inoue, K., Tanabe, Y., Lupski, J.R., 1999. Myelin deficiencies in both the central and the peripheral nervous systems associated with a SOX10 mutation. Annals of Neurology 46, 313–318.
Inoue, K., et al., 2004. Molecular mechanism for distinct neurological phenotypes conveyed by allelic truncating mutations. Nature Genetics 36, 361–369.
Kapoor, S., et al., 2012. Genetic analysis of an Indian family with members affected with Waardenburg syndrome and Duchenne muscular dystrophy. Molecular Vision 18, 2022–2032.
Madden, C., Halsted, M.J., Hopkin, R.J., Choo, D.I., Benton, C., Greinwald, J.H., 2003. Temporal bone abnormalities associated with hearing loss in Waardenburg syndrome. Laryngoscope 113, 2035–2041.
Oysu, C., Oysu, A., Aslan, I., Tinaz, M., 2001. Temporal bone imaging findings in Waardenburg's syndrome. International Journal of Pediatric Otorhinolaryngology 58, 215–221.
Pingault, V., et al., 1998. SOX10 mutations in patients with Waardenburg–Hirschsprung disease. Nature Genetics 18, 171–173.
Pingault, V., et al., 2002. SOX10 mutations in chronic intestinal pseudo-obstruction suggest a complex physiopathological mechanism. Human Genetics 111, 198–206.
Pingault, V., Ente, D., Dastot-Le Moal, F., Goossens, M., Marlin, S., Bondurand, N., 2010. Review and update of mutations causing Waardenburg syndrome. Human Mutation 31, 391–394.
Read, A.P., Newton, V.E., 1997. Waardenburg syndrome. Journal of Medical Genetics 34, 656–665.
Sham, M.H., Lui, V.C., Chen, B.L., Fu, M., Tam, P.K., 2001. Novel mutations of SOX10 suggest a dominant negative role in Waardenburg–Shah syndrome. Journal of Medical Genetics 38, E30.

RESEARCH ARTICLE

AMERICAN JOURNAL OF medical genetics PART A

Severe Congenital Lipodystrophy and a Progeroid Appearance: Mutation in the Penultimate Exon of *FBN1* Causing a Recognizable Phenotype

Toshiki Takenouchi,[1] Mariko Hida,[1] Yoshiaki Sakamoto,[2] Chiharu Torii,[3] Rika Kosaki,[4] Takao Takahashi,[1] and Kenjiro Kosaki[3]*

[1]Department of Pediatrics, Keio University School of Medicine, Tokyo, Japan

[2]Department of Plastic Surgery, Keio University School of Medicine, Tokyo, Japan

[3]Center for Medical Genetics, Keio University School of Medicine, Tokyo, Japan

[4]Division of Medical Genetics, National Center for Child Health and Development, Tokyo, Japan

Manuscript Received: 17 February 2013; Manuscript Accepted: 1 July 2013

Recently, three marfanoid patients with congenital lipodystrophy and a neonatal progeroid appearance were reported. Although their phenotype was distinct from that of classic Marfan syndrome, they all had a truncating mutation in the penultimate exon, i.e., exon 64, of *FBN1*, the causative gene for Marfan syndrome. These patients might represent a new entity, but the exact phenotypic and genotypic spectrum remains unknown. Here, we report on a girl born prematurely who exhibited severe congenital lipodystrophy and a neonatal progeroid appearance. The patient exhibited a characteristic growth pattern consisting of an accelerated growth in height with a discrepant poor weight gain. She had a characteristic facial appearance with craniosynostosis. A mutation analysis identified c.8175_8182del8bp, p.Arg2726Glufs*9 in exon 64 of the *FBN1* gene. A review of similar, recently reported patients revealed that the cardinal features of these patients include (1) congenital lipodystrophy, (2) premature birth with an accelerated linear growth disproportionate to the weight gain, and (3) a progeroid appearance with distinct facial features. Lines of molecular evidence suggested that this new progeroid syndrome represents a neomorphic phenotype caused by truncated transcripts with an extremely charged protein motif that escapes from nonsense-mediated mRNA decay, altering FBN1-TGF beta signaling, rather than representing the severe end of the hypomorphic phenotype of the FBN1-TGF beta disorder spectrum. We propose that this marfanoid entity comprised of congenital lipodystrophy, a neonatal progeroid appearance, and a peculiar growth profile and caused by rare mutations in the penultimate exon of *FBN1*, be newly referred to as marfanoid–progeroid syndrome. © 2013 Wiley Periodicals, Inc.

Key words: congenital lipodystrophy; progeroid appearance; Marfan syndrome

How to Cite this Article:
Takenouchi T, Hida M, Sakamoto Y, Torii C, Kosaki R, Takahashi T, Kosaki K. 2013. Severe congenital lipodystrophy and a progeroid appearance: Mutation in the penultimate exon of *FBN1* causing a recognizable phenotype.
Am J Med Genet Part A 161A:3057–3062.

INTRODUCTION

Recently, Graul-Neumann et al. [2010] reported a distinctive marfanoid patient with severe congenital lipodystrophy and a progeroid appearance arising from a truncating mutation in the penultimate exon, i.e., exon 64, of *Fibrillin (FBN)1* on 15q21.1, the causative gene for Marfan syndrome (OMIM 154700) [Graul-Neumann et al., 2010]. The documentation of two patients with a similar phenotype and mutation in the penultimate exon of the *FBN1* gene suggested that this *FBN1*-related progeroid syndrome represents a new disease entity [Goldblatt et al., 2011; Horn and Robinson, 2011]. These three patients presented with a progeroid appearance and arachnodactyly at birth. Their extreme thinness was distinctive from so-called neonatal Marfan syndrome, and none of the three patients had been diagnosed as such. All three patients were suspected of having an *FBN1* mutation based on the

Conflict of interest: none.
Grant sponsor: Ministry of Health, Labour and Welfare, Japan; Grant number: H23-013.
Abbreviations: FBN, fibrillin; NMD, nonsense-mediated mRNA decay; TGF, transforming growth factor.
*Correspondence to:
Kenjiro Kosaki, M.D., Center for Medical Genetics, Keio University School of Medicine, 35 Shinanomachi, Shinjuku-Ku, Tokyo 160-8582, Japan.
E-mail: kkosaki@z3.keio.jp
Article first published online in Wiley Online Library (wileyonlinelibrary.com): 16 August 2013
DOI 10.1002/ajmg.a.36157

emergence of some features of Marfan syndrome, including accelerated growth and subluxation of the lens, during adolescence. However, the striking progeroid appearance precluded a clinical diagnosis of Marfan syndrome. Two clinical questions remain to be elucidated: (1) what is the range of *FBN1* mutations that can be associated with this distinctive phenotype, and (2) what is the molecular basis of the phenotypic difference between classic Marfan syndrome and this presumably new disease entity.

Here, we document a young girl who had a distinctive neonatal progeroid presentation and a heterozygous mutation in exon 64 of *FBN1*. She had a previously undescribed critical feature, craniosynostosis, which is the hallmark of Shprintzen-Goldberg syndrome (OMIM182212) [Carmignac et al., 2012]. The documentation of craniosynostosis in this progeroid syndrome illustrates a phenotypic overlap among FBN1-transforming growth factor (TGF) beta signaling pathway disorders.

CLINICAL REPORT

The propositus was a Japanese girl born to non-consanguineous parents who did not have any family history of inherited conditions. The pregnancy was complicated by intrauterine growth retardation and oligohydramnios. The propositus was born at 34 and 3/7 weeks of gestation via emergency cesarean section for fetal tachycardia. The Apgar scores were 8 and 9 at 1 and 5 min, respectively. Her birth weight was 1,427 g (−2.3 SD), her length was 40 cm (−1.8 SD), and her head circumference was 30.6 cm (−0.3 SD). A physical examination at birth revealed a progeroid appearance, wide-open anterior fontanelle, low-set ears, long arms and legs, arachnodactyly, and arthrogryposis, especially in the lower extremities. During her hospital stay, she developed jaundice, for which she underwent phototherapy. She was noted to have a transient elevated blood pressure. A renal ultrasound showed mild right hydronephrosis with no evidence of vesico-ureteral reflex on a voiding cystogram. She continued to take lisinopril until the age of 2 years, when her blood pressure normalized.

During her infancy and childhood, she consistently had a poor weight gain, with a weight of 5.9 kg (−2.8 SD) at 1 year, 11.7 kg (−1.8 SD) at 4 years and 2 months, and 21.7 kg (−1.6 SD) at 10 years of age. There was a disproportionately accelerated height growth that is 70.9 cm (−0.8 SD) at 1 year, 107.6 cm (+1.5 SD) at 4 years and 2 months, and 148.9 cm (+1.9 SD) at 10 years of age (Fig. 1). As for her psychomotor development, she met all the developmental milestones without any delay and she attended a regular school. Standard blinded neuropsychological testing using the Japanese version of the Stanford–Binet test, i.e., the Tanaka–Binet test, indicated an intelligent quotient of 122 at the age of 5 years and 7 months. The presence of craniosynostosis and marfanoid features raised a clinical suspicion of Loeys–Dietz syndrome but an analysis of the *TGFBR1* and *TGFBR2* genes did not reveal any pathologic mutations.

On examination at 10 years of age, she was extremely thin with little palpable subcutaneous adipose tissue. Her body mass index was 9.8 kg/m^2 (−7.3 SD) [Inokuchi et al., 2007]. She had arachnodactyly, a progeroid appearance and scaphocephaly with a prominent forehead, proptosis, and pectus excavatum. Since she complained of a recent decline in her visual acuity, she underwent a detailed ophthalmologic examination that revealed bilateral severe myopia, and proptosis. There was no subluxation of the lenses. The optic discs were enlarged.

Imaging studies of her entire neuroaxis revealed craniosynostosis of the posterior portion of the sagittal suture (Fig. 2), mild enlargement of the ventricles (consistent with arrested hydrocephalus), and lumbosacral dural ectasia. An echocardiogram showed no enlargement of the sinus of Valsalva, allowing annuloaortic ectasia to be ruled out.

MOLECULAR ANALYSIS

Genomic DNA was extracted from a whole blood sample of the propositus. A mutation analysis panel (SureSelect XT-Auto custom; Agilent Technologies, Santa Clara, CA) was custom-designed to include most of the causative genes listed in the classic textbook of dysmorphology: *Smith's Recognizable Patterns of Human Malformation* [Jones, 2006] (the list of genes is available upon request). Sequencing of the propositus' PCR products using this custom-designed mutation analysis panel and a next-generation sequencer (MiSeq; Illumina, Inc., San Diego, CA) enabled a heterozygous 8 bp deletion to be identified, extending from nucleotides 8,175–8,182 relative to the adenine of the start codon in exon 64 of the *FBN1* gene that is c.8175_8182del8bp p.Arg2726Glufs*9. This mutation was predicted to result in a frame-shift truncation of the transcript encoded by exon 64 of *FBN1*. Sanger sequencing of the same PCR product amplified from exon 64 and flanking introns of *FBN1* with primer (forward: 5′-tcacaactgcaaggaacagg-3′, reverse: 5′-cttggaggaaaccacaggaa-3′) confirmed the heterozygous 8-bp deletion in exon 64 of *FBN1* gene.

DISCUSSION

Here, we document a patient with a heterozygous mutation in exon 64 of the *FBN1* gene with neonatal progeroid presentation. Her presentation was distinct from classic Marfan syndrome or neonatal Marfan syndrome, both of which are caused by an *FBN1* mutation. We concluded that this constellation of phenotypes represents a clinically recognizable entity with a common molecular basis.

We reviewed the detailed clinical characteristics of the four patients, including the propositus, in a tabular form (Table I). Three distinct clinical features were present in all the patients: (1) congenital lipodystrophy, (2) characteristic growth patterns with prematurity (range: 28–36 weeks of gestation), accelerated height growth that cross growth chart channels and a discrepant poor weight gain, and (3) a progeroid appearance with characteristic facial features including proptosis, downslanting palpebral fissures, and retrognathia. Mandatory features that overlap with those of Marfan syndrome included arachnodactyly, digital hyperextensibility, myopia, dural ectasia, and normal psychomotor development. We propose that these signs should represent the clinical diagnostic criteria for this condition, for which we propose to refer to as marfanoid–progeroid syndrome.

Apart from severe congenital lipodystrophy and a progeroid appearance, the presence of craniosynostosis in the context of marfanoid features overlaps with Shprintzen–Goldberg syndrome.

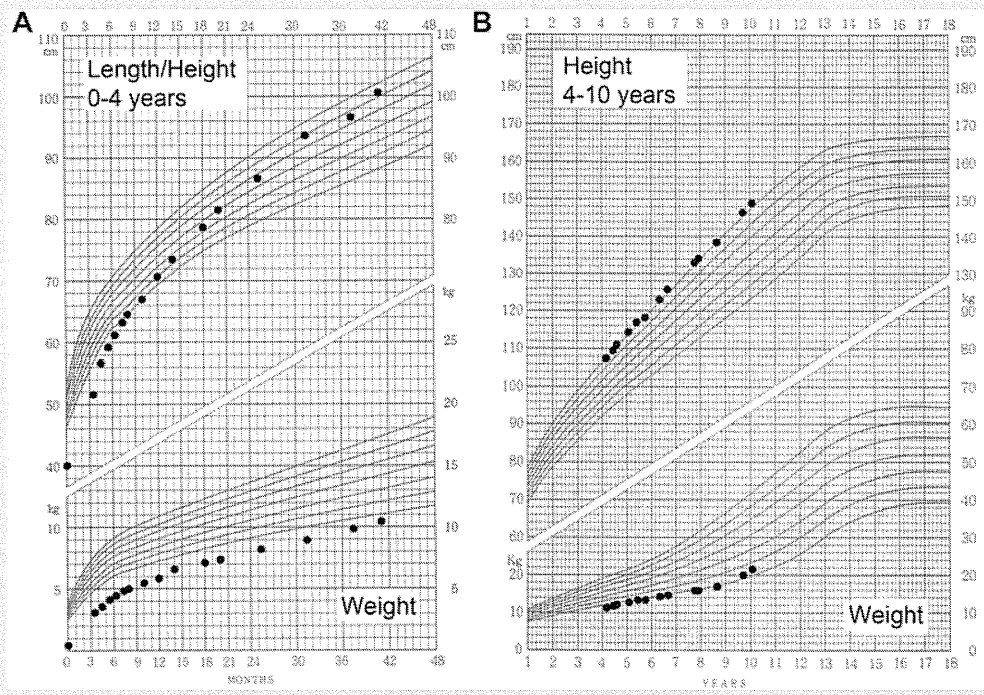

FIG. 1. Accelerated linear growth disproportionate to weight gain during childhood. Channels on the growth charts represent 3rd, 10th, 25th, 50th, 75th, 90th, and 97th centiles on the Japanese standard physical growth chart [Tsuzaki et al., 1987]. Note that the growth curve from birth to 48 months of age (A) shows a disproportionately accelerated height growth that crosses growth chart channels. The growth curve from 4 to 10 years of age (B) shows a poor weight gain that persisted throughout adolescence.

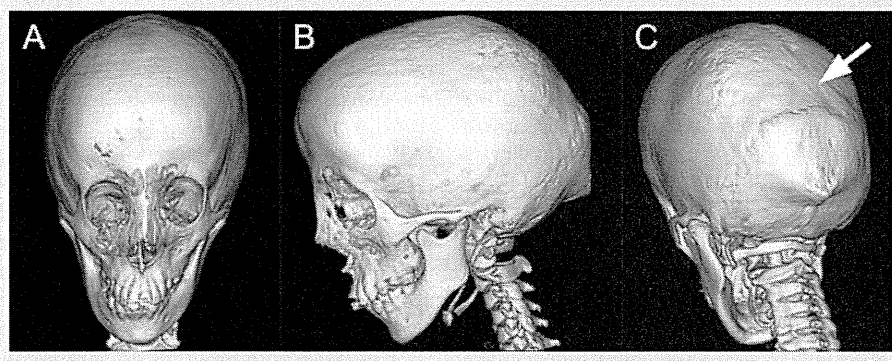

FIG. 2. Cranial computed tomography with three-dimensional reconstruction. Note the prominent forehead and marked scaphocephaly on the frontal view (A) and lateral view (B). A partial craniosynostosis of the posterior sagittal suture is visible (arrow, C).

This autosomal dominant disorder is caused by mutations in *SKI*, a repressor of the TGF beta signaling pathway, and is comprised of craniosynostosis, craniofacial abnormalities, and marfanoid features [Kosaki et al., 2006; Carmignac et al., 2012; Doyle et al., 2012]. It is notable that some patients with Loeys–Dietz syndrome (OMIM 609192), which is caused by a *TGFBR1* or *TGFBR2* mutation, can also present with craniosynostosis [Loeys et al., 2006]. The observation of craniosynostosis in these two classic syndromes and in the